

Regional trends in the fractional solubility of Fe and other metals North Atlantic aerosols (GEOTRACES cruises GA01 and GA03) following a two-stage leach

Rachel U. Shelley^{1,2,3}, William M. Landing¹, Simon J. Ussher², Helene Planquette³, and Geraldine Sarthou³

¹Dept. Earth, Ocean and Atmospheric Science, Florida State University, 117 N Woodward Ave, Tallahassee, Florida, 32301, USA

²School of Geography, Earth and Environmental Sciences, University of Plymouth, Drake Circus, Plymouth, PL4 8AA, UK

³Laboratoire des Sciences de l'Environnement Marin, UMR 6539 LEMAR (CNRS/UBO/IRD/IFREMER), Institut Universitaire Européen de la Mer, Technopôle Brest-Iroise, Plouzané 29280, France

Correspondence to: Rachel U. Shelley (rshelley@fsu.edu)

Abstract. The fractional solubility of aerosol-derived trace elements deposited to the ocean surface is a key parameter of many marine biogeochemical models. Yet, it is currently poorly constrained, in part due to the complex interplay between the various processes that govern the solubilisation of aerosol trace elements. In this study, we used a sequential two-stage leach to investigate the regional variability in fractional solubility of a suite of aerosol trace elements (Al, Ti, Fe, Mn, Co, Ni, Cu, Zn, Cd and Pb) from samples collected during three GEOTRACES cruises to the North Atlantic Ocean (GA01, GA03-2010 and GA03-2011). We present aerosol trace element solubility data from two sequential leaches that provide a “solubility window”, covering a conservative, lower limit to an upper limit, the maximum potentially soluble fraction, and discuss why this upper limit of solubility could be used as a proxy for the bioavailable fraction in some regions.

Regardless of the leaching solution used in this study (mild versus strong leach), the most heavily loaded samples generally had the lowest solubility. However, there were exceptions. Manganese fractional solubility was relatively uniform across the full range of atmospheric loading (32 ± 13 % and 49 ± 13 % for ultra-high purity water and 25 % acetic acid leaches, respectively). This is consistent with other marine aerosol studies. Zinc and Cd fractional solubility also appeared to be independent of atmospheric loading. Although the average fractional solubilities of Zn and Cd (Zn: 37 ± 28 % and 55 ± 30 %, Cd: 39 ± 23 % and 58 ± 26 % for ultra-high purity water and 25 % acetic acid leaches, respectively) were similar to Mn, the range was greater, with several samples being 100% soluble after the second leach. Finally, as the objective of this study was to investigate the regional variability in TE solubility, the samples were grouped according to air mass back trajectories (AMBTs). However, we conclude that AMBTs are not sufficiently discriminating to identify the aerosol sources or the potential effects of atmospheric processing on the physico-chemical composition and solubility of the aerosols.

40 **1. Introduction**

41 Aerosol trace element (TE) solubility is a key parameter of many biogeochemical models, but it is
42 poorly constrained, e.g. Fe solubility estimates range from 0.001-90 % (Aguilar-Islas et al., 2010;
43 Baker et al., 2016). The fractional solubility (herein referred to as “solubility”) of aerosol TEs is
44 defined in terms of the amount of a TE in solution from any given leach that passes through a filter
45 (usually < 0.45 or $0.2\ \mu\text{m}$), expressed as a percentage of the total (Baker and Croot, 2010; Baker et al.,
46 2016; Jickells et al., 2016). While this operational definition accounts for some of the variability in
47 published values, it does not account for all of it. A number of factors impact aerosol TE solubility,
48 such as: (1) the choice of leaching protocol, and (2) the aerosol source, which in turn is impacted by a
49 combination of factors such as the mineralogy of the particles, atmospheric processing during
50 transport, and the presence/absence of emissions from e.g. vehicles, industry and agricultural
51 practices. Several studies have concluded that the most significant effects on aerosol Fe solubility
52 result from the source/composition of the aerosols, rather than changes in physico-chemical
53 parameters, such as temperature, pH and oxygen concentration of the leach medium, or the choice of
54 batch versus flow-through techniques (e.g. Aguilar-Islas et al., 2010; Fishwick et al., 2014).

55 There have been a number of studies that have focused on the role of aerosol TEs on biogeochemical
56 cycles in the North Atlantic (e.g. Sarthou et al., 2003; Baker et al., 2013; Buck et al., 2010; Ussher et
57 al., 2013; Powell et al., 2015). More recently, the GEOTRACES programme has produced a number
58 of aerosol datasets, which has stimulated further discussion on the use of this data to look for trends
59 that link TE solubility and aerosol source (e.g. Baker et al., 2016; Jickells et al., 2016). Elemental
60 ratios, enrichment factors and air mass back trajectory simulations have long been used as a first
61 approximation of aerosol source, and there are many studies that employ multivariate statistical
62 analyses for aerosol source apportionment (e.g. Chueinta et al., 2000; Laing et al., 2015). In addition,
63 more studies are making use of stable isotope ratios to investigate aerosol provenance. Some of these
64 methods are well-established and have a relatively long history of use in this purpose, such as Pb
65 isotopes (e.g. Maring et al., 1987), and Sr and Nd isotopes (e.g. Skonieczny et al., 2011; Scheuven et
66 al., 2013 and references therein), and data from investigations of novel isotope systems are increasing.
67 For example, Fe isotopes show promise as a way to differentiate between anthropogenic and mineral
68 dust aerosols (Conway et al., submitted). In contrast, Cd isotopes may not be a suitable tool for aerosol
69 source apportionment (Bridgestock et al., 2017).

70 As the soluble fractions of aerosol TEs are thought to be the most-readily bioavailable forms (Shaked
71 and Lis, 2009), the leachable (soluble) fraction is used as a first approximation of the bioavailable
72 fraction. Therefore, experimental conditions should mimic natural conditions as closely as possible,
73 while yielding reproducible results. Ideally, the leach protocol used fits both these criteria. However,
74 that is not always strictly possible for reasons such as access to the leach medium of choice,

75 availability of analytical instrumentation, and cost. Currently, however, there is no standardised
76 aerosol leaching protocol, but it is recognised that this should be a priority for future studies (Baker et
77 al., 2016). Some commonly-used leach media are ultra-high purity (UHP) water (18.2 MΩ.cm),
78 seawater, weak acids (e.g. 1% HCl, 25 % acetic acid), or ammonium acetate buffer (e.g. Buck et al.,
79 2006, Baker et al., 2006b; Berger et al., 2008).

80 To investigate the regional variation in the solubility of key TEs in the North Atlantic, aerosol samples
81 were collected during the US-GEOTRACES GA03 campaigns in 2010 and 2011, and the French
82 GEOTRACES GA01 campaign in 2014 (www.geotraces.org). The focus of this paper is Fe and the
83 GEOTRACES “key” trace elements, Al, Cd, Cu, Mn, Pb, Zn, plus Co, Ni, and Ti (GEOTRACES
84 Planning Group, 2006). This suite of TEs includes bioactive elements, tracers of atmospheric
85 deposition, and elements characteristic of anthropogenic aerosols. Some TEs fit into more than one of
86 these categories. Here, we use the term ‘trace element’ in the context of open ocean water column
87 concentrations, thus acknowledging that elements such as Al, Fe and Ti are not present in trace
88 concentrations in aerosol source material. Aerosol concentrations for a suite of other elements (Li, Na,
89 Mg, P, Sc, V, As, Se, Rb, Sr, Sn, Sb, Cs, Ba, La, Ce, Nd, Th, U) were also determined, but will not be
90 discussed further here. However, these data are available at BCO-DMO (GA03; www.bco-dmo.org/)
91 and LEFE-CYBER (GA01; (www.obsvlf.fr/proof/php/GEOVIDE/GEOVIDE.php), and on request
92 from the lead author.

93 In this study a two-stage leach protocol was followed. the first leach employed was the
94 “instantaneous” leach described by Buck et al. (2006) which is a flow-through method where the leach
95 medium is in contact with the aerosols for 10 - 30 s. It can be conducted using UHP water or seawater.
96 The advantages of using UHP water are that UHP water is a reproducible medium (allowing for inter-
97 lab comparisons) that can easily be analysed by ICP-MS for many elements simultaneously without
98 the need for time-consuming sample handling steps such as separation techniques and drying down
99 then re-dissolving the residue. Leaches with UHP water can be conducted at sea, or in the home
100 laboratory. If fresh sea water is used the leaches must be undertaken at sea.

101 Given that UHP water and rain water have broadly similar pH (~ pH 5.6), UHP water is used as an
102 analogue for rain/wet deposition, as wet deposition is thought to dominate the supply of many TEs, at
103 least at some regional and local scales (Helmers and Shremms, 1995; Kim et al., 1999; Powell et al.,
104 2015). However, the extremely low ionic strength of UHP water, and the absence of the metal binding
105 ligands naturally present in rain water and seawater (e.g. Chieze et al., 2012; Wozniak et al., 2014),
106 means that UHP water is not a perfect analogue for oceanic receiving waters. As such, freshly-
107 collected, filtered (< 0.2 μm) seawater likely produces a better estimate of the fractional solubility of
108 TEs on first contact with oceanic receiving waters. For Fe, leaches using UHP water (~ pH 5.6)

typically produce higher solubility estimates than leaches conducted with natural seawater (~ pH 8.2) due to the pH sensitivity of dissolution and the higher ionic strength of sea water. On occasions where higher solubility in seawater is observed, complexation by Fe binding ligands is likely the cause. Regardless of whether UHP water or seawater is used, the instantaneous leach likely yields conservative lower limit estimates of TE solubility due to the short contact time between the aerosols and leach medium, and reports that aerosol solubility has a bi-modal behaviour for many TEs (initial fast release, followed by a slower sustained release with time; e.g. Desboeufs et al. 2005; Kocak et al., 2007; Mackey et al., 2015).

The second, sequential leach was employed in order to estimate an upper limit of TE solubility, and provide a “solubility window”, but also as an estimate of the maximum bioavailable fraction during the residence time of aerosol particles in the euphotic zone. We used the 25 % acetic acid leach with hydroxylamine hydrochloride described by Berger et al. (2008). The pH of this leach (pH 2.1) is just below that of zooplankton or fish digestive tracts and the reducing agent mimics the low oxygen environments inside faecal pellets and marine snow aggregates. Indeed, Schmidt et al. (2016) have demonstrated that lithogenic Fe is mobilised in the gut passage of krill resulting in threefold higher Fe content in the muscle, and fivefold higher Fe content of the faecal pellets of specimens close to lithogenic source material compared to those from offshore.

2. Methods

2.1. Aerosol sample collection

Aerosol samples (n = 57) were collected aboard the *R/V Knorr* during the *US-GEOTRACES GA03* cruises (15 Oct – 2 Nov 2010 and 6 Nov – 9 Dec 2011, and aboard the *N/O Pourquoi Pas?* during the French GEOTRACES GA01 cruise (GEOVIDE, 15 May – 30 June 2014) (Fig. 1). Both campaigns took place in the North Atlantic Ocean, with GA03-2010 and GA01 departing from Lisbon, Portugal. The cruise tracks were designed to traverse a wide variety of biogeochemical provinces (Longhurst, 2010) including; continental shelf regions, an eastern boundary current upwelling system (off West Africa), the oligotrophic North Atlantic gyre, and sub-Arctic waters, and to span a large gradient in atmospheric dust loading. The aerosol collections have been described previously (Wozniak et al., 2013; 2014; Shelley et al., 2015; 2017). Briefly, air was simultaneously pulled through twelve acid-washed 47 mm diameter Whatman 41 (W41) ashless filter discs at approximately $1.2 \text{ m}^3 \text{ min}^{-1}$ (134 cm s^{-1} face velocity) using a high-volume aerosol sampler (TSP model 5170V-BL, Tisch Environmental). The metadata and concentration data for the aerosol leaches can be found in the supplementary information (Table S1). All filters were stored frozen (-20°C) and double bagged prior to processing, both on the ship and upon returning to the home laboratories. To avoid contamination from the ship’s stack exhaust, aerosol sampling was controlled with respect to wind sector and wind speed using an anemometer interfaced with a datalogger (CR800, Campbell

Scientific). The samplers were programmed to run when the wind was $\pm 60^\circ$ from the bow of the ship and $> 0.5 \text{ m s}^{-1}$. When the wind failed to meet these two criteria, the motors were shut off automatically and not allowed to restart until the wind met both the speed and direction criteria for 5 continuous minutes. In addition, the samplers were deployed on the ship's flying bridge as high off the water as possible ($\sim 14 \text{ m}$ above sea level) to minimise collection of sea spray.

2.2. Trace element determination – totals aerosol TEs

The total digestion method of Morton et al. (2013) was used for the determination of total aerosol TE loadings (Al, Ti, Mn, Fe, Co, Ni, Cu, Zn, Cd, Pb). The W41 filter discs were digested in tightly-capped 15 mL Teflon-PFA vials (Savillex). Firstly, 1000 μL of ultrahigh purity (UHP) 15.8 M nitric acid (Optima or Merck Ultrapur) was added to each vial, heated to 150°C on a hotplate, and then taken to dryness. Secondly, 500 μL of 15.8 M nitric acid (13.2 M HNO_3) and 100 μL of 28.9 M hydrofluoric acid (5.8 M HF) (Optima or Merck Ultrapur) was added to each vial, re-heated to 150°C on a hotplate, then taken to near dryness. After the final digestion and evaporation step, the samples were re-dissolved in 20 mL of 0.32 M nitric acid for analysis. All filter digestions were performed under Class-100 laminar flow conditions. Total aerosol TE concentrations were determined by magnetic sector field inductively coupled plasma mass spectrometry (ICP-MS; Thermo Element-2) at the National High Magnetic Field Laboratory (NHMFL) at Florida State University (FSU; GA03) or Pôle de Spectrométrie Océan (PSO) at the Institut Universitaire Européen de la Mer, France (IUEM; GA01). Samples were introduced to a PFA-ST nebuliser (Elemental Scientific Inc.) via a modified SC-Fast introduction system consisting of an SC-2 autosampler, a six-port valve and a vacuum rinsing pump. Replicate blank solutions for the acid digestions were prepared by digesting W41 discs that had been deployed in the aerosol samplers for 1 h while not in operation, and the resulting concentrations were subtracted from all acid-digested filter samples. Details of the digestion blanks and analytical figures of merit, including CRM recoveries, have previously been reported (Shelley et al., 2015; 2017).

2.3. Trace element determination – soluble aerosol TEs

In this study, we used a two-step, sequential leach to investigate regional variation in aerosol sources, TE fractional solubility and bioavailability. We discuss the results from (1) an 'instantaneous' leach (Buck et al., 2006), that provides a lower limit estimate of the most labile TE fraction (analogous to the initial rapid release of TEs into rain drops and the surface mixed layer of the ocean), followed by (2) a more protracted leach using 25 % acetic acid (with the reducing agent, hydroxylamine hydrochloride, and heat, 10 min at 90°C), which mimics the slower and sustained release from aerosol particles during their residence time in the euphotic zone.

179 The first step, the “instantaneous” leach, was conducted under a Class-100 laminar flow hood. In this
 180 technique, 100 mL of UHP water ($> 18 \text{ M}\Omega\cdot\text{cm}$ resistivity, $\text{pH} \sim 5.5$, Barnstead Nanopure) is rapidly
 181 passed through an aerosol-laden W41 filter held in a polysulfone vacuum filtration assembly
 182 (Nalgene). Operationally-defined dissolved ($\leq 0.45 \mu\text{m}$) TEs are collected in the filtrate (leachate) by
 183 positioning a GN-6 Metrice backing filter (cellulose esters) below the W41 disc in the filtration
 184 assembly (Buck et al., 2006). In this study, the leachate was transferred to an acid-clean low density
 185 polyethylene (LDPE) bottle and acidified to 0.024 M ($\sim \text{pH} 1.7$) with UHP HCl and double-bagged for
 186 storage until analysis at FSU or IUEM. As for total elemental determinations, soluble TEs in the
 187 leachate were also determined by ICP-MS. Leachate blanks were prepared by passing 100 mL of UHP
 188 water through W41 filters that had been deployed in the aerosol sampler for 1 h while not in operation.
 189 For example, leachate blanks for Fe represented an average of $1.6 \pm 0.4 \%$ and $15.5 \pm 15.8 \%$ of the Fe
 190 sample concentrations for GA03 and GA01, respectively). A subset of samples (GA03-2011) were
 191 also leached using the instantaneous leach procedure with freshly collected, filtered ($0.2 \mu\text{m}$) seawater
 192 as the leach medium. Leachate blanks were subtracted from all leachate sample concentrations, details
 193 of which can be found in Table S1 in the Supplementary Material.

194

195 The UHP water fractional solubility was calculated using Eq. (1):

$$\frac{[\text{element}]_{\text{UHP water leach}}}{[\text{element}]_{\text{total}}} * 100 = \text{UHP water Fractional Solubility} \quad (1)$$

198 Following the instantaneous UHP water leach, the filter was transferred to a 15 mL centrifuge tube,
 199 and the second leach was undertaken, using 5 mL of 25 % (4.4 M) ultrapure acetic acid, with 0.02 M
 200 hydroxylamine hydrochloride as the reducing agent (Berger et al., 2008). After a 10 min heating step
 201 (90°C), the leaches were left for 24 h before being centrifuged for 5 min at 3400xg. The leachate was
 202 then carefully decanted into acid-clean LDPE bottles. In order to rinse any residual acetic acid from
 203 the filter, 5 mL of UHP water was pipetted into the centrifuge tubes, which were then centrifuged
 204 again for 5 min at 3400xg. This supernatant was then added to the acetic acid leachate in the LDPE
 205 sample bottles. As this second leach aims to access a less labile fraction of the TEs of interest
 206 (including TEs absorbed to surfaces, TE oxyhydroxides and TEs complexed by aerosol organic
 207 matter), without significantly attacking TEs bound within the mineral matrix (Koçak et al., 2007;
 208 Berger et al., 2008), it may provide an upper limit estimate for the fractional solubility of these aerosol
 209 TEs as the aerosols mix down into the ocean. There is a slight risk that the heating step could begin to
 210 attack the mineral matrix, resulting in a slight over-estimation of the upper limit of solubility, but this
 211 risk was shown to be minimal (Berger et al., 2008). Despite this risk, the heating step was included
 212 because of the desire for procedural similarity with marine particle leaches from the same cruises (e.g.
 213 Planquette et al., 2016; H. Planquette and A. Gourain pers. comm.), which have been used to assess

the relative importance of atmospheric inputs of TEs to water column concentrations of Al, Fe and Pb (Menzel-Baraqueta et al.; Tonnard et al.; Zurbrick et al., this issue).

As all samples in this study were leached first using the UHP water instantaneous leach, followed by a sequential leach with 25 % acetic acid, the overall solubility in 25% acetic acid was calculated using Eq. (2):

$$\frac{[element]_{UHP\ water\ leach}}{[element]_{total}} + \frac{[element]_{25\ \% \ HAc\ leach}}{[element]_{total}} * 100 = HAc\ Fractional\ Solubility \quad (2)$$

2.4. Major anion determination

Before the UHP water leachate was acidified, a 10 mL aliquot was taken from each leach sample for the determination of the soluble major anions. The aliquot was immediately frozen for storage. The anions, Cl^- , NO_3^- and SO_4^{2-} , were determined by ion chromatography using either a Dionex 4500i (at FSU for GA03 samples) or a Metrohm, IC850 system (at Laboratoire Interuniversitaire des Systèmes Atmosphériques, Paris for GA01 samples).

2.5. Air mass back trajectory simulations

Air mass back trajectory (AMBT) simulations were generated using the publicly-available NOAA Air Resources Laboratory Hybrid Single-Particle Lagrangian Integrated Trajectory (HYSPLIT) model, using the GDAS meteorology (Stein et al., 2015; Rolph, 2017). The 5-day AMBT simulations were used to describe five regional categories, based on the predominant trajectories for the air masses. The simulations and further details of these categories can be found in Wozniak et al., (2013; 2014) and Shelley et al., (2015; 2017). Briefly, for cruise GA03 air masses were characterised as European, North American, North African, or Marine (no or minimal interaction with major continental land masses within the 5-day simulation period). For cruise GA01, all the samples were classified as High Latitude dust (originating north of 50°N; Bullard et al., 2016). The classifications are shown in Table S1, and the AMBT simulations from Shelley et al. (2015; 2017) have been reproduced and can be found in the Supplementary Material (Fig. S1). The simulations use arrival heights of 50, 500 and 1500 m, so that at least one height was located in the marine boundary layer.

3. Results and Discussion

3.1. Identifying aerosol provenance

Air mass back trajectory (AMBT) simulations are frequently used to identify the origin and/or flow path of air masses, from which a first approximation of aerosol provenance (e.g. deserts, urban regions, or biomass burning) are made. While a useful tool in oceanographic studies, AMBTs used

247 alone do have limitations. Perhaps the most significant of these is that they are unable to quantify the
248 contribution of different aerosol types or the entrainment of particles along the flow path of the air
249 mass. Indeed, within the five categories described in this study multiple sources are likely to have
250 contributed to the composition of the bulk aerosol of each category. This study is likely to be
251 particularly sensitive to this as the sampling site was not static (i.e. sampling occurred along three
252 different transects), and air masses can, and do, take different pathways within a general wind
253 direction. Consequently, AMBTs are not adequately discriminating for aerosol source apportionment.
254 However, we have organised the data using the AMBT categories as the objective of this study was to
255 look for trends in solubility at a regional level, and also for consistency with our earlier published
256 work from the North Atlantic (Wozniak et al., 2013; 2014; Shelley et al., 2015; 2017).

257 More powerful approaches for aerosol source apportionment consider the physico-chemical
258 composition of the aerosols, either as the bulk aerosol or individual particles. There have been a
259 number of field campaigns (e.g. DABEX, DODO, SAMUM and AMMA) and individual studies
260 which have provided a wealth of information about the physico-chemical composition of African dust
261 before, during and after long-range transport (e.g. Johansen et al., 2000; Johnson et al., 2008;
262 McConnell et al., 2008; Petzold et al., 2009; Marticorena et al., 2010; Trapp et al., 2010; Formenti et
263 al., 2011). These studies, and satellite data have identified the key dust source regions in North Africa
264 (Prospero et al., 2002). Chemical composition data for other aerosol end members which supply
265 aerosols to the North Atlantic is not as extensive, but some examples of individual studies and field
266 campaigns can be found in Table S2. In addition, campaigns in the Atlantic Ocean which have
267 sampled marine aerosols (e.g. Atlantic Meridional Transect, CLIVAR, GEOTRACES) have identified
268 aerosol sources from characteristic groups of elements and elemental ratios (e.g. high concentrations
269 of lithogenic elements are characteristic of a mineral dust, K is a tracer of biomass burning, and
270 correlations between V and Ni are diagnostic of emissions from marine shipping; Baker et al., 2006a;
271 Sippula et al., 2014; Baker and Jickells, 2017), organic compounds (e.g. Wozniak et al., 2013; 2014,
272 2015), and/or stable isotopic signatures (Scheuvens et al., 2013 and references therein).

273 Although atmospheric inputs to the ocean are episodic and exhibit a seasonality in the tropical and
274 subtropical North Atlantic that is largely driven by the migration of the intertropical convergence zone
275 (Prospero et al., 1981; Adams et al., 2012; Doherty et al., 2014), North African/Saharan mineral dust
276 dominated the aerosol composition in the GA03 study region (Conway and John, 2014; Shelley et al.,
277 2015; Conway et al., submitted). Other aerosol sources in Europe and North America and sea salt also
278 contributed to the bulk aerosol to varying extents. In contrast to GA03, the GA01 transect was located
279 north of the extent of the Saharan dust plume ($\sim 25^\circ$ N in summer, Ben-Ami et al., 2009), and was
280 thus influenced by a mixture of high latitude dust sources (Prospero et al., 2012; Shelley et al., 2017),
281 which also have a seasonal cycle. As a result, a large dynamic range of aerosol loading was observed

282 (Fe = 0.185–5650 ng m⁻³; Al = 0.761- 7490 ng m⁻³) during these two campaigns, with the highest Fe
283 and Al loadings associated with the North African samples (GA03), lower loadings with the Marine
284 samples (GA03), and the lowest loadings observed in the samples collected in the Labrador Sea
285 (GA01).

286 Total Fe and Al were strongly correlated ($r^2 = 0.999$, Pearson's $p < 0.01$), demonstrating that the two
287 metals have common lithogenic source(s) (Fig. 2). However, this correlation was largely driven by the
288 heavily-loaded North African samples ($r^2 = 0.997$, $P < 0.01$). For each of the other source categories,
289 simple linear regression of the data resulted in r^2 values of: 0.879 ($P < 0.01$) for High Latitude dust
290 (GA01), 0.890 ($P = 0.057$) for European samples (GA03), 0.983 ($P = 0.34$) for N. American samples
291 (GA03) and 0.751 ($P = 0.70$) for Marine samples (GA03) (Fig. 2b). Further discussion of sub-regional
292 differences in the Fe/Al ratio are addressed later in the Discussion. For the other TEs, strong
293 correlations for the combined GA01 and GA03 datasets were found between Ti/Al ($r^2 = 0.999$, $P <$
294 0.01), Mn/Al ($r^2 = 0.994$, $P < 0.01$) and Co/Al ($r^2 = 0.996$, $P < 0.01$), in accord with previous
295 observations in this region owing to the primarily lithogenic sources of these elements (e.g. Jickells et
296 al., 2016). The correlations between Al and the primarily anthropogenic TEs, Ni, Cu, Zn, Cd, and Pb,
297 were also significant at the 99% confidence level : Ni/Al ($r^2 = 0.884$), Cu/Al ($r^2 = 0.652$), Pb/Al ($r^2 =$
298 0.478), Zn/Al ($r^2 = 0.321$), Cd/Al ($r^2 = 0.303$) due the presence of the heavily-loaded North African
299 samples, which accounted for between 88 % and 30 % of the statistical variance for Ni and Cd,
300 respectively. Sources other than mineral dust (e.g. metal smelting emissions, fly ash, vehicle
301 emissions, volcanic ash, proglacial till) are presumably responsible for the residual variance.
302 Establishing the contributions from these other aerosol sources and their influence on TE solubility is
303 a research priority.

304 As the aerosol source has a direct bearing on the type and composition of aerosols, determining the
305 source could provide useful data that might be used to predict the fractional solubility of aerosol TEs.
306 As positive matrix factorisation (PMF) can be used for source apportionment, we used the USA
307 Environmental Protection Agency's EPA PMF model (v. 5.0) with the total TE concentration data to
308 look for trends in the data. However, the GA01 and GA03 dataset is relatively small ($n = 57$) and the
309 model was not stable with more than two factors. The two factors were a mineral dust factor (high
310 contributions from lithogenic TEs, in particular Al, Ti, Fe and Zr) and a pollution/anthropogenic factor
311 (with high contributions from Zn and Pb) (Fig. S2a, Supplementary Material). As anticipated, the
312 mineral dust factor dominated where North African aerosols were sampled, and the pollution factor
313 was relatively more important closer to the European and North American continents (Fig. S2b). This
314 is in accord with the samples from North Africa having elemental mass ratios that are consistently the
315 closest to the UCC elemental ratios compared to aerosols from the other source regions (Fig. 3). In
316 the High Latitude samples, the pollution factor and the mineral dust factor were of approximately

equal dominance. Interestingly, the North African aerosols also contained a relatively strong pollution component, consistent with a northeast flow into North Africa from Europe, followed by entrainment of mineral dust during passage over the Sahara (Baker and Jickells, 2017). Given that the PMF indicates that 100 % of the variability in the Cd concentrations was explained by the pollution factor, this suggests that Cd in North African aerosols is not sourced from mineral dust, which would explain why no fractionation was observed in Cd isotopes from North African and European aerosols (Bridgestock et al., 2017). Further, it also suggests that even the relatively homogeneous aerosols from North Africa do not represent a ‘pure’ end-member. However, the PMF analysis was not sensitive enough to identify the full complement of aerosol sources contributing to the samples collected during GA01 and GA03.

3.2. Elemental mass ratios and aerosol source

Elemental mass ratios from the ten most heavily loaded GA03 North African aerosols were averaged to derive a value for the ‘North African’ ratio depicted by the dashed horizontal line in Figures 3(a-i). Aluminium was used to normalise the data (Fig. 3; Table S2) and was chosen instead of Ti, another proxy for mineral dust, due to the presence of some anomalously high Ti/Al ratios in some of the Marine samples during GA03 (Fig. 3a; Shelley et al., 2015). We have previously reported a mass ratio of 0.76 for Fe/Al for the North African end-member aerosols (Shelley et al., 2015; Fig. 2a), which is significantly higher than the mean upper continental crustal (UCC) ratio of 0.47 (Rudnick and Gao, 2003) but entirely consistent other studies of Saharan soils and dust (e.g. Chiapello et al., 1997; Guieu et al., 2002; Lafon et al., 2006; Baker et al., 2013).

For North African dust there does not appear to be a discernible source dependent trend in Fe/Al ratios due to a natural variability in Fe-bearing minerals in soils in dust source regions (Lafon et al., 2006; Scheuven et al., 2013), but it might be possible to use Fe/Al ratios for some of the other aerosol groups to suggest different sources. For example, the European samples ($n = 4$) fall into two sub-groups: two samples have low Fe/Al ratios (Fig. 2; E3 = 0.48, E4 = 0.10 and Fig. 3c), whereas the other two samples (E1 = 0.95 and E2 = 0.78) have Fe/Al ratios within the range of the North American samples (Fe/Al 1.1 ± 0.22 , range 0.86-1.42) and all but one of the Marine samples (Fe/Al, excluding M12, 0.93 ± 0.33 , range 0.59-1.61; M12, collected closest to the North African samples, Fe/Al = 0.43).

Aerosols from the more northerly section, GA01, were largely outside the influence of the Saharan dust plume (Shelley et al., 2017), and are all classified as High Latitude in this study (Fig. 3). For this group of samples, there were also sub-groups of Fe/Al ratios. During the first half of the cruise (Fig. 1), there was a group of samples (G1-6, G8 and G10) with Fe/Al ratios of 0.58 ± 0.05 ; Fig.3c). This is intermediate between the UCC ratio (0.48 ± 0.07) and the North African mineral dust ratio ($0.78 \pm$

0.03; Fig. 3c). For these samples, the wind direction was predominantly from the north/north west (Shelley et al., 2017), so it is unlikely that the observed ratios reflect a mixture of North African mineral dust and European aerosols. Rather, it more likely comes from high latitude sources, as dust supplied by proglacial till from Iceland and Greenland peaks in spring/early summer, and can be deposited over the Atlantic Ocean (Prospero et al., 2012; Bullard et al., 2016). Unfortunately, the extensive cloud cover experienced during the GA01 cruise (May/June 2014) prevented the use of satellite observations (e.g. <http://worldview.earthdata.nasa.gov>) which would have confirmed the presence of dust from these sources. The elemental ratios calculated from TE concentrations from volcanic ash sampled during the eruption of the Eyjafjallajökull volcano in 2010 (Achterberg et al., 2013) offers some limited support for this argument, as our range of elemental ratios encompasses this end-member (Icelandic soils are almost exclusively volcanic in origin; Arnalds 2004). However, although Icelandic sands (Baratoux et al., 2011) and tephra (Oladottir et al., 2011) have Mn/Al ratios that overlap the GA01 samples, Fe/Al is generally lower in our High Latitude dust samples (Table S2).

A second group of GA01 samples (G7, G9, G11 and G12) had Fe/Al ratios of 0.34 ± 0.01 , but no obvious link in terms of the AMBTs. The Greenland shelf and Labrador Sea samples, except G15, had low Fe/Al (0.16 ± 0.04), and were distinct from those collected on the Canadian shelf (0.48 ± 0.02). These trends strongly suggest that the High Latitude dust was made up of at least four aerosol sources.

While there is evidence for anthropogenic source(s) of aerosol Fe to the North Atlantic (Conway et al., submitted), which is more soluble than Fe associated with mineral dust (Sedwick et al., 2007; Sholkovitz et al., 2009; 2012), North African mineral dust dominates the supply of Fe to much of the study region (Baker et al., 2013; Shelley et al., 2015; 2017; Conway et al., submitted). In addition to the samples classified as European and North American, elevated Fe/Al ratios were also observed in the Marine samples (Fig. 2b). In addition to aerosols derived from continental sources (meaning either mineral dust or anthropogenic emissions), sea spray aerosols could make a relatively higher contribution to the bulk aerosol in remote oceanic locations (de Leeuw et al., 2014). However, this would have the opposite effect as the ratio of Fe/Al in surface seawater ($0.017 - 0.024$ in the North Atlantic gyre, 0.019 European continental shelf, and $0.030 - 0.031$ in the Mauritanian upwelling zone; Hatta et al., 2015) is two orders of magnitude lower than the crustal ratio. Hence the contribution of sea spray aerosols appears to have a negligible impact on the Fe/Al ratios in the bulk Marine aerosols.

The Marine, and the High Latitude samples had the widest range in Fe/Al ratios and were also collected in the most remote locations. These groups also had the greatest difference in the Fe/Al ratios between the total and soluble fractions, and also contained the samples with the lowest ratios of Fe/Al in the soluble fraction (minimum Fe/Al = 0.15 , samples G9-GA01 and M3-GA03; Fig. 3c), suggesting that even though aerosol Fe is altered towards more soluble forms during atmospheric

transport (Longo et al., 2016), atmospheric processing renders Al even more soluble relative to Fe. However, although the soluble ratio of Fe/Al was the same for samples G9-GA01 and M3-GA03, the fractional solubility for Fe differed from 20 % for G9-GA01 to 0.8 % for M3-GA03. We suggest that North African mineral dust was contributing to the composition of M3-GA03, resulting in the low solubility of Fe compared to G9-GA01. This suggestion is supported by isotopic evidence (Conway et al., submitted).

For the anthropogenically-derived TEs, Ni, Cu, Zn, Cd and Pb (Figs. 3e-i) and for at least some of samples of the mixed-source TEs (i.e. having crustal and pollution sources; e.g. Mn and Co in Figs. 3b and d), there is some degree of source-dependence in the elemental ratios, with some significant increases from the UCC mass ratios in the total (Shelley et al., 2015) and UHP water soluble fractions (Fig. 3). The higher ratios of the UHP water soluble fraction compared to the total indicates that these TEs are more labile than Al. In addition, studies that have investigated the size distribution of aerosols have found that anthropogenically-derived TEs tend to be associated with fine mode aerosols ($< 1 \mu\text{m}$ diameter), which are more soluble than coarse mode aerosols due to the larger surface area to volume ratio (Duce et al., 1991; Baker and Jickells 2006; Baker and Jickells, 2017). Size fractionated samples were collected during the GA03 cruise, and the smaller size fractions were indeed more soluble than the larger ones for Al, Fe and Co (Landing and Shelley, 2013). Enrichment of TEs with predominantly anthropogenic sources accords with other studies in the North Atlantic, and is most striking for aerosols that did not originate from the sparsely-populated, arid regions of North Africa (e.g. Buck et al., 2010; Gelado-Cabellero et al., 2012; Patey et al., 2015; Shelley et al., 2015).

3.3. Aerosol solubility

3.3.1. Solubility of aerosol TEs as a function of total concentration: UHP water (instantaneous) compared to 25 % acetic acid leaches

The UHP water soluble fraction of aerosol Fe and Al determined for all the North Atlantic GA01 and GA03 samples varied by two orders of magnitude (Fig. 4a: Fe = 0.14 - 21 %, median 2.2 %; Al = 0.34 - 28 %, median 2.7%). Although a broader range of Fe and Al solubility was observed in this study, both these results and those reported by Buck et al. (2010) using the same approach (Fe = 2.9 - 47%, median = 14%, and Al = 3.7 - 50%, median = 9.5%) broadly agree that the median UHP water soluble fractions of Fe compared to Al in the North Atlantic are similar. While there was considerable overlap in the ranges of fractional solubility of TEs in aerosols from the different regions (e.g. Fe: European 1.9 – 21 %; N. American 0.84 – 8.8 %; Marine 1.7 – 18 %; High Latitude dust 1.9 – 20 %), the North African samples, identified by their orange colour, high Fe and Al loadings, and definitive AMBTs formed a distinct cluster of very poorly soluble Fe, or Al ($< 1\%$; Fig. 4a). However, the solubility of the North African ('Saharan') aerosol Fe was 1 – 2 orders of magnitude lower in this study (0.14 –

0.57 %) than during the Buck et al. (2010) study (2.9 – 19 %). This supports the hypothesis that TEs from North African aerosols sampled closer to the source (as in this study) are less soluble due to a lesser degree of atmospheric processing and/or larger particle sizes (Baker and Jickells, 2006; Longo et al., 2016).

The inverse relationship between total aerosol loading and fractional solubility has previously been reported for Fe (Sholkovitz et al., 2009; 2012; Jickells et al., 2016) and Al (Jickells et al., 2016). Jickells et al. (2016) compiled solubility data from the North Atlantic and found that the general trend between Fe and Al solubility and atmospheric loading was robust over the range of atmospheric loadings found in the North Atlantic, regardless of the leach protocol employed. In this study, both the UHP soluble, and 25 % acetic acid soluble fractions of Fe and Al (Figs 4a and b) were related to atmospheric loading, i.e. the highest loaded North African samples had the lowest solubility. The possible exception to this trend is the fraction of Al that dissolved from North African aerosols following the 25 % acetic acid leach (Fig. 4b). However, it could simply be that we are observing scatter in our data, which is smoothed out in the larger dataset ($n > 2000$) examined by Jickells et al. (2016). Although we cannot rule out that this effect is the result of the heating step in the 25 % acetic acid leach attacking the alumino-silicate matrix, the similarity in the trend of the solubility of Ti in UHP water and 25 % acetic acid (sharp decrease in solubility with increased aerosol loading, Figs. 4a and b) suggests that matrix attack is minimal. Further experimentation with and without the heating step would help to clarify this issue.

Aluminium, Ti, and Fe show very similar behaviour in Figure 4a (sharply decreasing solubility as loading increases). Cobalt, Ni, Cu, Zn and Pb solubilities decrease less strongly as loading increases, whereas Mn and Cd show no clear trend. For the acetic acid leaches (Fig. 4b), Ti follows the same trend as the UHP water leach (Fig. 4a), while Al and Fe plateau at 8-10 % solubility. The other TEs (Mn, Co, Ni, Cu, Zn, Cd and Pb) all show almost no trend with loading. The absence of an inverse trend between solubility and loading has previously been noted for Mn (Jickells et al., 2016). For Co the inverse relationship between UHP water solubility and loading was not observed when using the 25 % acetic acid leach, most likely because Co may be associated with the Mn and Fe oxides that are easily reduced using this leach. For Zn and Cd, although their average fractional solubilities (Zn: 37 ± 28 % and 55 ± 30 %, Cd: 39 ± 23 % and 58 ± 26 % for ultra-high purity water and 25 % acetic acid leaches, respectively) were similar to Mn (32 ± 13 % and 49 ± 13 % for ultra-high purity water and 25 % acetic acid leaches, respectively), the range was greater, with several samples from different regions (although not North Africa) being 100% soluble after the second leach.

3.3.2. Solubility of TEs: UHP water (instantaneous) compared to 25 % acetic acid leaches

All ten TEs from the five different categories were less soluble in UHP water than 25 % acetic acid (Fig. 5). This is not a surprising finding given the lower pH of acetic acid compared with UHP water, acetate being a bidentate ligand, the longer contact time of the aerosols with the leach solution, the addition of the hydroxylamine reducing agent and that the fractional solubility of TEs in 25 % acetic acid was calculated using Equation 2 (which sums the UHP water and 25 % acetic acid leach concentrations). In addition, there is some degree of source-dependent variability in the relative proportions of each TE that is released by the two leaches. In general, as with the leaches with UHP water, the North African aerosols were distinctly less soluble in 25% acetic acid compared with aerosols from the other source regions (Fig. 5). Figure 5 highlights the distinction between the lithogenic elements, Al, Fe and Ti, which have uniformly low solubility in UHP water (mostly < 20 %), and extremely low solubility in North African aerosols (< 1 %), and the anthropogenic, pollution-dominated elements, Ni, Cu, Zn, Cd and Pb which have solubility up to 100 %. Manganese and Co have both lithogenic and anthropogenic sources, so are classified as “mixed-source”, and have intermediate solubilities. Like all the TEs reported here, Mn solubility in UHP water was significantly less ($p < 0.01$, two-tailed, homoscedastic t-test) in North African aerosols (median solubility = 19 %) than in the non-North African samples (median = 38%), which seems to contrast somewhat with the findings of Baker et al. (2006b) and Jickells et al. (2016) which found that aerosol source had little impact on Mn solubility. However, in common with these earlier studies (Baker et al., 2006b; Jickells et al., 2016), there was no significant source-dependent difference in Mn solubility in 25 % acetic acid (non-North African samples: $49 \pm 15\%$, North African samples: $49 \pm 6.4\%$).

3.3.3. Soluble TEs: UHP water compared to seawater instantaneous leaches

Seawater leaches were conducted on a subset of samples (GA03-2011), to investigate the suitability of seawater as the leach medium in the instantaneous leach (Fig. 6). During this study, Fe solubility in seawater was lower than in UHP water (Fig. 6c). This phenomenon has previously been observed in atmospheric aerosols from the North Atlantic Ocean (Buck et al., 2010). For Fe, only a few samples of North American and Marine provenance conformed to the relationship described by the equation proposed by Buck et al. (2010), with most of our data plotting above the regression line of the Buck et al. (2010) study (Fig. 6c), indicating that our data was relatively more soluble in UHP water compared to seawater than in this earlier study. One possibility is that the higher aerosol Fe loadings we observed during GA03-2011 (this study, maximum = $5650 \text{ ng Fe m}^{-3}$), compared to the A16N-2003 transect (Buck et al. 2010; maximum = $1330 \text{ ng Fe m}^{-3}$), resulted in a particle concentration effect (Baker and Jickells, 2006), whereby the relationship between aerosol Fe loading and fractional solubility breaks down because dust on the filter can be a source of soluble Fe but can also scavenge dissolved Fe from the sea water leach solution as it passes through the filter. Given that the link between Fe solubility in seawater and Fe-binding ligand availability is well established (e.g. Rue and

488 Bruland, 1995; Gledhill and Buck, 2012), an alternative explanation for the difference in Fe solubility
489 is that the organic composition of the seawater used as the leach mediums differed between the two
490 studies.

491 Manganese is the only TE that had a slope close to unity (0.98; Fig. 6b), suggesting that solubility
492 estimates were not impacted by the choice of leach medium used. This is consistent with other studies
493 that have found that Mn solubility is less sensitive to the choice of leach media, or to aerosol
494 provenance than other TEs (Baker et al., 2006b; Jickells et al., 2016). Due to the large variability in
495 the data set, there was no significant difference between Mn solubility in UHP water or seawater ($32 \pm$
496 13% and $24 \pm 17 \%$, respectively; Fig. S3 and Tables S3 and S4, Supplementary Material). Table S5
497 shows which regions had slopes for UHP water versus seawater fractional solubility that did not differ
498 significantly from 1.0 at the 95 % confidence level (t-statistic).

499 Lead was the only TE with all slopes differing significantly from 1.0, and the only TE where the
500 solubility in seawater was higher than in UHP water for virtually every sample (Fig. 6i). As for Pb,
501 most of the Co data falls below the 1:1 line (Fig. 6d), indicating that Co was also generally more
502 soluble in seawater than UHP water. In contrast, the opposite trend was observed for Fe and Ni (Figs
503 6c and e), perhaps due to differences in the availability of metal binding ligands in the seawater used.
504 A challenge of using seawater as the leach medium is that it is difficult to control for natural
505 variability in the types and concentrations of organic ligands. Consequently, it is not possible to
506 determine conclusively why contrasting trends in the fractional solubility of TEs were observed. For
507 this reason, we advocate for the use of UHP water as a common leach medium to facilitate
508 comparisons of solubility resulting from differences in aerosol composition. An additional benefit is
509 the ease of analysis of UHP water compared to seawater.

510

511 **3.4. Visualising marine aerosol sources using multivariate statistical approaches**

512 As the PMF analysis was only able to identify two significant factors accounting for the total aerosol
513 TE concentrations, another multivariate approach was taken. Hierarchical cluster analysis (Ward's
514 method, Euclidian distance) was performed using the R statistical package (v. 3.3.0; R Core Team,
515 2016) to look for trends in the data that might reveal the various aerosol sources. Hierarchical cluster
516 analysis was performed on (1) log transformed total aerosol TE plus NO_3^- concentration data (Fig. 7a),
517 and (2) log transformed TE fractional solubility plus NO_3^- concentration data (Fig. 7b). The NO_3^-
518 concentrations appear in both runs as we wanted to include TEs plus an indicator of anthropogenic
519 pollution.

Figure 7a shows two main branches to the dendrogram of the total TE concentration data. One branch groups all the North African and European samples and two North American samples (N2 and N4) together, and the other branch groups all other samples together. Samples closest to each other are the most similar to each other, and those joined in the same groups share similar characteristics. Therefore, in this analysis, the North African samples are grouped together, as are the High Latitude samples. All but three North African samples form a distinct sub-group. The three remaining North African samples (A8, A9 and A11) share more characteristics with the European samples, lending support for mixing of aerosols from the two regions. Counterintuitively, the two European samples with the lowest Fe/Al ratios (E3 and E4) are the ones that are most similar to the two North American samples, which have relatively high Fe/Al ratios of 0.90 and 0.87. The GA01 samples (with the exception of one sample, G15) form a distinct cluster, but with three sub-groups: one is the Greenland/Labrador Sea samples (without G15), and the other two are related to each other but distinct from the Greenland/Labrador Sea samples and are a mixture geographically of the other samples. However, there is a trend, the 'middle' group is the group of samples collected closest to land, the group to the right is the group of samples collected furthest from land. The other groupings are made up of a mixture of North American and Marine samples. This suggests that the Marine samples are comprised predominantly of North American aerosols from more than one source. The only anomaly is the two North American samples that 'look European'.

Although there are differences between Figures 7a (total TEs) and 7b (25 % acetic acid fractional solubility; Eq. 2), the general trend of an inverse relationship between TE atmospheric loading and fractional solubility holds, as the North African samples with the highest concentrations and lowest fractional solubilities appear on the left in Figure 7a, and on the right in Figure 7b. In terms of fractional solubility, the N. African samples form a distinct cluster, but this cluster is made up of two sub-groups: one collected during GA03-2010 and one during GA03-2011. The samples collected from near Greenland and the Labrador Sea are also distinct from the other GA01 samples (again with the exception of G15), and also distinct from all other samples. The European samples, all other GA01 samples, and three North American samples form a loose cluster. The remaining North American samples and all the Marine samples form another loose cluster.

Plotting the data this way still does not allow us to identify the aerosol sources definitively, but it does allow us to visualise which samples have the most similar physico-chemical characteristics and confirms the general trend of a relationship between aerosol loading and fractional solubility and, by extension, bioavailability, even though we have demonstrated that this relationship is not present for all TEs. This knowledge is then useful as a general rule of thumb in biogeochemical models, although clearly other factors also exert controls on aerosol TE solubility. For example, during their investigations of the GA03 aerosols, Wozniak et al., (2013; 2014; 2015) proposed a role for water

soluble organic carbon (WSOC) in controlling the solubility of Fe. Desboeufs et al. (2005) also found evidence for a link between total carbon and TE solubility in regions impacted by anthropogenic activity. Thus, the carbon content of aerosols is also implicated as a control on aerosol Fe solubility, but the relationship is frequently not linear.

559

3.5. Choice of leach and modelling TE solubility

The ability of models to replicate subtleties in aerosol TE solubility may prove critical in forecasting ecosystem impacts and responses. Due to the magnitude of North African dust inputs to the North Atlantic region (very high dust inputs result in a high soluble TE aerosol flux despite relatively low fractional solubility), this is a particular challenge and is compounded by additional unknowns such as how aerosol acidity will be impacted by the combined effects of increasing industrialisation/urbanisation, and changes in the magnitude of future mineral dust supply and biomass burning (Knippertz et al., 2015; Weber et al., 2016). In other words, it is important to accurately constrain aerosol TE solubility with high quality data in order to improve the predictive capacity of models. Clearly the choice of leach media and protocol impacts the measured fractional solubility. This is shown in both Figures 4 and 5 and has a number of implications with regard to modelling the impact of atmospheric deposition on marine biogeochemistry. For example, for elements with generally low solubility, such as Fe, the difference between 1 % and 2 % solubility is an increase of 100 %, meaning that only half the amount of dust is needed to yield the same amount of dissolved Fe. To complicate matters further, recent research has demonstrated that some diazotrophs are able to directly access particulate Fe (Rubin et al., 2011). The significance of this is that *Trichodesmium* are common in the North Atlantic gyre under the influence of the Saharan plume, and the North African dust samples have higher fractional solubility for Fe using the acetic acid leach. If *Trichodesmium* are able to access the acetic acid soluble fraction of the aerosol Fe, as the study indicates (Rubin et al., 2011), our data suggests that twentyfold more aerosol Fe is available for uptake than is suggested from the instantaneous UHP water leach. This suggests that in regions where *Trichodesmium* proliferate, we are likely to underestimate bioavailable Fe using the instantaneous UHP water leaching method.

There are implications for modelling the impact of atmospheric deposition for other TEs. Although, the lack of source dependent differences in Mn solubility in these aerosols makes modelling Mn solubility simpler, there was still a difference in the fractional solubility calculated from the two leaches (UHP water: 32 ± 13 % and 25 % acetic acid: 49 ± 13 %). However, for Al, there was a large range in solubility: 0.3 – 28 % using UHP water and 4.1 – 100 % using 25 % acetic acid. Both ranges far exceed the relatively narrow range used in the MADCOW model (1.5 – 5 %), which has been used to estimate atmospheric inputs based on dissolved Al concentrations in the mixed layer (Measures and

589 Brown, 1996). It is noted, however, that the median values from this study fall within the range used
590 by the MADCOW model (2.7 % and 3.3 % for UHP water and 25 % acetic acid, respectively). We
591 highlight this issue to draw attention to some of the problems inherent in modelling TE solubility and
592 its impact on the chemistry and biogeochemistry of the upper ocean.

593 Given that the different leaching approaches access different fractions of aerosol TEs that can dissolve
594 from aerosols at different rates (e.g. TEs loosely bound to surfaces and TEs that are associated with
595 less reactive phases) (e.g. Kocak et al., 2007; Mackey et al., 2015), we need to conduct experiments
596 that elucidate the relationship between the soluble and bioavailable fractions. In the meantime, we
597 suggest that the 25 % acetic acid leach might be better to estimate the bioavailable fraction given that
598 Fe (and perhaps other TEs) associated with lithogenic particles are directly available to micro-
599 organisms in productive regions and regions with high dust inputs (Rubin et al., 2011) and that aerosol
600 particles can be processed by zooplankton (Schmidt et al., 2016).

601

602 **4. Conclusions**

603 Aerosol TE solubility is usually determined using operationally-defined methods, while
604 biogeochemical models require robust relationships between two or more parameters that can be used
605 to predict TE solubility in order to constrain the bioavailable fraction of aerosol TEs. In this study, we
606 used a two-stage leach (UHP water followed by 25 % acetic acid with hydroxylamine hydrochloride)
607 to investigate the fractional solubility of a suite of trace elements (Al, Ti, Mn, Fe, Co, Ni, Cu, Zn, Cd,
608 Pb) from aerosols collected in the North Atlantic during three GEOTRACES research cruises (GA03-
609 2010, GA03-2011 and GA01). Five regions were identified based on air mass back trajectory (AMBT)
610 simulations; i) North Africa, ii) Europe, iii) North America, iv) High Latitude, and v) Marine.
611 However, the AMBTs were not able to sufficiently discriminate aerosol sources within these regions.
612 Of these five categories, the North African aerosols were the most homogeneous in terms of their
613 fractional solubility and elemental ratios. In contrast, samples from the most remote locations, the
614 Marine and High Latitude aerosols, had the most spread in their fractional solubility and elemental
615 ratios. Elemental ratios were discussed rather than enrichment factors normalised to UCC composition
616 since earlier work highlighted that the UCC ratios are not representative of the North African mineral
617 dust end-member, which dominates aerosol supply in much of the study area.

618 We observed an inverse relationship between the fractional solubility of Al, Ti, Fe, Ni, Cu and Pb and
619 aerosol loading for all leach media (UHP water, filtered seawater, and 25 % acetic acid with
620 hydroxylamine hydrochloride). However, Mn, Zn and Cd fractional solubility appears to be
621 independent of atmospheric loading. For Co, the inverse relationship between UHP water solubility
622 and loading was not observed when using the 25 % acetic acid leach, most likely because Co may be

623 associated with the Mn and Fe oxides that are easily reduced using the 25 % acetic acid leach. Further
624 work is required to assess exactly which fraction is accessed by the various leach protocols in order to
625 understand links between the soluble and bioavailable fractions.

626

627 **Data availability**

628 Data is available at BCO-DMO (GA03; www.bco-dmo.org) and LEFE-CYBER (GA01;
629 (www.obsvlfr.fr/proof/php/GEOVIDE/GEOVIDE.php), and on request from the lead author.

630 **Acknowledgements**

631 Many thanks to the captains and crews of the RV Knorr (GA03-2010 and 2011) and NO Pourquoi
632 Pas? (GA01), the chief scientists (GA03 = Bob Anderson, Ed Boyle, Greg Cutter; GA01 = Geraldine
633 Sarthou and Pascale Lherminier), Alex Baker for the loan of the aerosol sampler used on GA01, and
634 Alina Ebling Petroc Shelley, Alex Landing and Sarah Huff for their help with sample processing and
635 analysis. This work was supported by grants to WML (NSF-OCE 0752832, 0929919 and 1132766),
636 and GS (ANR-13-B506-0014 and ANR-12-PDOC-0025-01). RUS was supported by a LabexMER
637 International Postdoctoral Fellowship and CG29 Postdoctoral Fellowship. A portion of this work was
638 performed at the National High Magnetic Field Laboratory, which is supported by National Science
639 Foundation Cooperative Agreement No. DMR-1157490 and the State of Florida. The aerosol
640 digestions for GA01 were undertaken in the geochemistry clean room at Ifremer (Centre de Bretagne).
641 Trace element determination for GA01 was conducted at the Pôle de Spectrométrie Océan at the
642 Institut Universitaire Européen de la Mer with the support and guidance of Claire Bollinger and
643 Marie-Laure Rouget. Finally, we thank Karine Desbeoufs and an anonymous reviewer for their
644 critiques that have contributed to the improvement of this manuscript.

645

646 **References**

- 647 Achterberg, E. P., Moore, C.M., Henson, S. A., Steigenberger, S., Stohl, A., Eckhardt, S., Avendano,
648 LC., Cassidy, M., Hembury, D., Klar, J.K., Lucas, M.I., Macey, A.I., Marsay, C.M., and, Ryan-
649 Keogh, T.J.: Natural iron fertilization by the Eyjafjallajökull volcanic eruption, *Geophys. Res. Lett.*,
650 40, 921-926, <http://doi.org/10.1002/grl.50221>, 2013.
- 651 Adams, A. M., Prospero, J.M., and Zhang, C.: CALIPSO-Derived Three-Dimensional Structure of
652 Aerosol over the Atlantic Basin and Adjacent Continents, *Journal of Climate*, 25, 6862-6879,
653 <http://doi.org/10.1175/JCLI-D-11-00672.1>, 2012.
- 654 Aguilar-Islas, A. M., Wu, J., Rember, R., Johansen, A.M. and Shank, L. M.: Dissolution of aerosol-
655 derived iron in seawater: Leach solution chemistry, aerosol type, and colloidal iron fraction, *Marine*
656 *Chemistry*, 120, 25-33., 2010.
- 657 Arnalds, O.: Soils of Iceland, *Jökull*, 58, 409-421, 2004.

658 Baker, A. R., Adams, C., Bell, T.G., Jickells, T.D., and Ganzeveld, L.: Estimation of atmospheric
659 nutrient inputs to the Atlantic Ocean from 50N to 50S based on large-scale filed sampling: Iron and
660 other dust-associated elements, *Global Biogeochem. Cycles*, 27, 755-767,
661 <http://doi.org/10.1002/gbc.20062>, 2013, 2013.

662 Baker, A. R., and, Croot, P. L.: Atmospheric and marine controls on aerosol iron solubility in
663 seawater., *Marine Chemistry*., 120, 4-13, 2010.

664 Baker, A. R., and Jickells, T.D.: Mineral particle size as a control on aerosol iron solubility., *Geophys.*
665 *Res. Lett.*, 33, <http://doi.org/10.1029/2006GL026557>, 2006.

666 Baker, A. R., and, Jickells, T.D.: Atmospheric deposition of soluble trace elements along the Atlantic
667 Meridional Transect (AMT), *Progress in Oceanography*, 158, 41-51, [10.1016/j.pocean.2016.10.002](https://doi.org/10.1016/j.pocean.2016.10.002),
668 2017.

669 Baker, A. R., Jickells, T. D., Biswas, K. F., Weston, K., and French, M.: Nutrients in atmospheric
670 aerosol particles along the Atlantic Meridional Transect, *Deep Sea Research Part II: Topical Studies in*
671 *Oceanography*, 53, 1706-1719, 2006a.

672 Baker, A. R., Jickells, T. D., Witt, M., and Linge, K. L.: Trends in the solubility of iron, aluminium,
673 manganese and phosphorus in aerosol collected over the Atlantic Ocean, *Marine Chemistry*, 98, 43-58,
674 2006b.

675 Baker, A. R., Landing, W.M., Bucciarelli, E., Cheize, M., Fietz, S., Hayes, C.T., Kadko, D., Morton,
676 P.L., Rogan, N., Sarthou, G., Shelley, R.U., Shi, Z., Shiller, A., and, van Hulten, M.M.P.: Trace
677 element and isotope deposition across the air–sea interface: progress and research needs, *Philosophical*
678 *Transactions of the Royal Society A: Mathematical, Physical and Engineering Sciences*, 374,
679 <http://doi.org/10.1098/rsta.2016.0190>, 2016.

680 Baratoux, D., Mangold, N., Arnalds, O., Bardintzeff, J.-M., Platevoët, B., Grégoire, M., and Pinet, P.:
681 Volcanic sands of Iceland - Diverse origins of aeolian sand deposits revealed at Dyngjúsandur and
682 Lambahraun, *Earth Surf. Process. Landforms*, 36, 1789-1808, [10.1002/esp.2201](https://doi.org/10.1002/esp.2201), 2011.

683 Ben-Ami, Y., Koren, I., Rudich, Y., Artaxo, P., Martin, S.T., and Andreae, M.O.: Transport of North
684 African dust from the Bodele depression to the Amazon Basin: a case study, *Atmos. Chem. Phys.*, 10,
685 7533-7544, <http://doi.org/10.5194/acp-10-7533-2010>, 2010.

686 Berger, J. M., Lippiatt, S.M., Lawrence, M.G., and Bruland, K.W.: Application of a chemical leach
687 technique for estimating labile particulate aluminum, iron, and manganese in the Columbia River
688 plume and coastal waters off Oregon and Washington., *Journal of Geophysical Research*, 113,
689 <http://doi.org/10.1029/2007JC004703>, 2008.

690 Bridgestock, L., Rehkämper, M., van de Flierdt, T., Murphy, K., Khondoker, R., Baker, A. R., Chance,
691 R., Strekopytov, S., Humphreys-Williams, E., and Achterberg E.P.: The Cd isotope composition of
692 atmospheric aerosols from the Tropical Atlantic Ocean, *Geophys. Res. Lett.*, 44, 2932-2940,
693 <http://doi.org/10.1002/2017GL072748>, 2017.

694 Buck, C. S., Landing, W.M., and Resing, J.: Pacific Ocean aerosols: Deposition and solubility of iron,
695 aluminum, and other trace elements, *Marine Chemistry*, 157, 117-130,
696 <http://dx.doi.org/10.1016/j.marchem.2013.09.005>, 2013.

697 Buck, C. S., Landing, W.M., Resing, J. A., Lebon, G. T.: Aerosol iron and aluminum solubility in the
698 northwest Pacific Ocean: Results from the 2002 IOC cruise, *Geochemistry, Geophysics, Geosystems.*,
699 7, <http://doi.org/10.1029/2005GC000977>, 2006.

700 Buck, C. S., Landing, W.M., Resing, J.A. and Measures, C.I.: The solubility and deposition of aerosol
701 Fe and other trace elements in the North Atlantic Ocean: Observations from the A16N CLIVAR/CO₂
702 repeat hydrography section., *Marine Chemistry.*, 120, 57-70, 2010.

703 Bullard, J. E., Baddock, M., Bradwell, T., Crusius, J., Darlington, E., Gaiero, D., Gassó, S.,
704 Gisladottir, G., Hodgkins, R., McCulloch, R., McKenna-Neuman, C., Mockford, T., Stewart, H., and,
705 Thorsteinsson, T.: High-latitude dust in the Earth system, *Reviews of Geophysics*, 54, 447-485,
706 <http://doi.org/10.1002/2016RG000518>, 2016.

707 Cheize, M., Sarthou, G., Croot, P., Bucciarelli, E., Baudoux, A.-C., and Baker, A.: Iron organic
708 speciation determination in rainwater using cathodic stripping voltammetry, *Analytica Chimica Acta*,
709 726, 45-54, 2012.

710 Chiapello, I., Bergametti, G., Chatenet, B., Bousquet, P., Dulac, F., and Soares, E. S.: Origins of
711 African dust transported over the northeastern tropical Atlantic, *Journal of Geophysical Research:*
712 *Atmospheres*, 102, 13701-13709, [10.1029/97jd00259](http://doi.org/10.1029/97jd00259), 1997.

713 Chueinta, W., Hopke, P. K., and Paatero, P.: Investigation of sources of atmospheric aerosol at urban
714 and suburban residential areas in Thailand by positive matrix factorization, *Atmospheric Environment*,
715 34, 3319-3329, [http://dx.doi.org/10.1016/S1352-2310\(99\)00433-1](http://dx.doi.org/10.1016/S1352-2310(99)00433-1), 2000.

716 Conway, T. M., and John, S.G.: Quantification of dissolved iron sources to the North Atlantic Ocean,
717 *Nature*, 511, 212-215, <http://doi.org/10.1038/nature13482>. 2014.

718 Conway, T.M., Shelley, R.U., Aguilar-Islas, A.M., Landing, W.M., Mahowald, N.M., and John, S.G.:
719 Iron isotopes reveal and important anthropogenic aerosol iron flux to the North Atlantic. Submitted to:
720 *Nature Communications*.

721 de Leeuw, G., Guieu, C., Arneth, A., Bellouin, N., Bopp, L., Boyd, P.W., Denier van der Gon, H.A.C.,
722 Desboeufs, K.V., Dulac, F., Facchini, M.C., Gantt, B., Langmann, B., Mahowald, N.M., Maranon, E.,
723 O'Dowd, C., Olgun, N., Pulido-Villena, E., Rinaldi, M., Stephanou, E.G., and Wagener, T. : Ocean-
724 atmosphere interactions of particles, in: *Ocean-atmosphere interactions of gases and particles*, edited
725 by: Liss, P. S., and Johnson, M.T., Springer-Verlag, Berlin, 171-245, 2014.

726 Desboeufs, K. V., Sofikitis, A., Losno, R., Colin, J. L. and Ausset, P.: Dissolution and solubility of
727 trace metals from natural and anthropogenic aerosol particulate matter., *Chemosphere*, 58, 195-203.,
728 2005.

729 Doherty, O. M., Riemer, N., and Hameed, S.: Role of the convergence zone over West Africa in
730 controlling Saharan mineral dust load and transport in the boreal summer, *Tellus B*, 66,
731 <http://doi.org/10.3402/tellusb.v66.23191>, 2014.

732 Fishwick, M. P., Sedwick, P.N., Lohan, M.C., Worsfold, P.J., Buck, K.N., Church, T.M., and Ussher,
733 S.J.: The impact of changing surface ocean conditions on the dissolution of aerosol iron, *Global*
734 *Biogeochem. Cycles*, 28, 1235-1250, <http://doi.org/10.1002/2014GB 004921>, 2014.

735 Gelado-Caballero, M. D., López-García, P., Prieto, S., Patey, M.D., Collado, C., Hernández-Brito, J.J.:
 736 Long-term aerosol measurements in Gran Canaria, Canary Islands: Particle concentration, sources and
 737 elemental composition, *Journal of Geophysical Research: Atmospheres*, 117, D03304,
 738 <http://doi.org/10.1029/2011jd016646>, 2012.

739 GEOTRACES Planning Group, GEOTRACES Science Plan. Baltimore, Maryland:
 740 Scientific Committee on Oceanic Research, <http://www.geotraces.org/science/science-plan>, 2006.

741 Gledhill, M., and Buck, K. N.: The organic complexation of iron in the marine environment: a review,
 742 *Frontiers in Microbiology*, <https://doi.org/10.3389/fmicb.2012.00069>, 2012.

743 Hatta, M., Measures, C. I., Wu, J., Roshan, S., Fitzsimmons, J. N., Sedwick, P., and, and Morton, P.:
 744 An overview of dissolved Fe and Mn Distributions during the 2010–2011 U.S. GEOTRACES north
 745 Atlantic Cruises: GEOTRACES GA03, Deep Sea Research Part II: Topical Studies in Oceanography,
 746 <http://dx.doi.org/10.1016/j.dsr2.2014.07.005>, 2015.

747 Helmers, E., and Schrems, O.: Wet deposition of metals to the tropical North and the South Atlantic
 748 Ocean, *Atmospheric Environment*, 29, 2475-2484, 1995.

749 Jickells, T. D., Baker, A. R., and Chance, R.: Atmospheric transport of trace elements and nutrients to
 750 the oceans, *Philosophical Transactions of the Royal Society A: Mathematical, Physical and*
 751 *Engineering Sciences*, 374, <http://doi.org/10.1098/rsta.2015.0286>, 2016.

752 Jickells, T. D., An, Z.S., Andersen, K.K., Baker, A.R., Bergametti, G., Brooks, N., Cao, J.J., Boyd,
 753 P.W., Duce, R.A., Hunter, K.A., Kawahata, H., Kubilay, N., laRoche, J., Liss, P.J., Mahowald, N.,
 754 Prospero, J.M., Ridgwell, A.J., Tegen, I., and Torres, R.: Global iron connections between desert dust,
 755 ocean biogeochemistry and climate., *Science*, 308, 67-71, 2005.

756 Johansen, A., Siefert, R.L., Hoffmann, M.R.: Chemical composition of aerosols collected over the
 757 tropical North Atlantic Ocean, *Journal of Geophysical Research*, 105, 15277-15312, 2000.

758 Johnson, B. T., Osborne, S.R., Haywood, J.M., and Harrison, M.A.J.: Aircraft measurements of
 759 biomass burning aerosol over West Africa during DABEX, *J. Geophys. Res.*, 113,
 760 [10.1029/2007JD009451](http://doi.org/10.1029/2007JD009451), 2008.

761 Kim, G., Alleman, L.Y., and Church, T.M.: Atmospheric depositional fluxes of trace elements, ²¹⁰Pb,
 762 and ⁷Be to the Sargasso Sea, *Global Biogeochemical Cycles*, 13, <http://doi.org/10.1029/1999gb900071>, 1999.

764 Knippertz, P., Coe, H., Chiu, J. C., Evans, M.J., Fink, A.H., Kalthoff, N., Lioussé, C., Mari, C.,
 765 Allan, R.P., Brooks, B., Danour, S., Flamant, C., Jegede, O.O., Lohou, F., and, Marsham, J.H.: The
 766 DACCWA Project: Dynamics–Aerosol–Chemistry–Cloud Interactions in West Africa, *Bulletin of the*
 767 *American Meteorological Society*, 96, 1451-1460, [10.1175/BAMS-D-14-00108.1](http://doi.org/10.1175/BAMS-D-14-00108.1), 2015.

768 Koçak, M., Kubilay, N., Herut, B., and Nimmo, M.: Trace Metal Solid State Speciation in Aerosols of
 769 the Northern Levantine Basin, East Mediterranean, *Journal of Atmospheric Chemistry*, 56, 239-257,
 770 <http://doi.org/10.1007/s10874-006-9053-7>, 2007.

771 Lafon, S., Sokolik, I. N., Rajot, J. L., Caquineau, S. and Gaudichet, A.: Characterization of iron oxides
 772 in mineral dust aerosols: Implications for light absorption, *J. Geophys. Res.*, 111,
 773 [10.1029/2005JD007016](http://doi.org/10.1029/2005JD007016), 2006.

774 Laing, J. R., Hopke, P.K., Hopke, E.F., Husain, L., Dutkiewicz, V.A., Paatero, J., and Viisanen, Y.:
775 Positive Matrix Factorization of 47 Years of Particle Measurements in Finnish Arctic, Aerosol and Air
776 Quality Research, 15, 188-207, <http://doi.org/10.4209/aaqr.2014.04.0084>, 2015.

777 Landing, W.M., and Shelley, R.U.: Particle size effects on aerosol iron solubility from the U.S.
778 GEOTRACES North Atlantic Zonal Transect (2010, 2011), ASLO 2013 Aquatic Sciences Meeting,
779 2013.

780 Longhurst, A.: Ecological Geography of the Sea., Academic Press., San Diego, 1998.

781 Longo, A. F., Feng, Y., Lai, B., Landing, W.M., Shelley, R.U., Nenes, A., Mihalopoulos, N., Violaki,
782 K., and, Ingall, E.D.: Influence of Atmospheric Processes on the Solubility and Composition of Iron in
783 Saharan Dust, Environmental Science & Technology, 50, 6912-6920,
784 <http://doi.org/10.1021/acs.est.6b02605>, 2016.

785 Mackey, K. R. M., Chien, C.-T., Post, A.F., Saito, M.A., and Paytan, A.: Rapid and gradual modes of
786 aerosol trace metal dissolution in seawater, Frontiers in Microbiology, 5, 1-11,
787 <http://doi.org/10.3389/fmicb.2014.00794>, 2015.

788 Maring, H., Settle, D.M., Buat-Ménard, P., Dulac, F., and, Patterson, C.C.: Stable lead isotopes tracers
789 of air mass trajectories in the Mediterranean region, Nature, 300, 154-156, 1987.

790 Marticorena, B., Chatenet, B., Rajot, J. L., Traoré, S., Coulibaly, M., Diallo, A., Koné, I., Maman, A.,
791 Ndiaye, T., and Zakou, A.: Temporal variability of mineral dust concentrations over West Africa:
792 analyses of a pluriannual monitoring from the AMMA Sahelian Dust Transect, Atmos. Chem. Phys.,
793 10, 8899-8915, [10.5194/acp-10-8899-2010](https://doi.org/10.5194/acp-10-8899-2010), 2010.

794 McConnell, C. L., Highwood, E.J., Coe, H., Formenti, P., Anderson, B., Osborne, S., Nava, S.,
795 Desboeufs, K., Chen, G., and Harrison, M.A.J.: Seasonal variations of the physical and optical
796 characteristics of Saharan dust: Results from the Dust Outflow and Deposition to the Ocean (DODO)
797 experiment, Journal of Geophysical Research: Atmospheres, 113, D14S05, [10.1029/2007jd009606](https://doi.org/10.1029/2007jd009606),
798 2008.

799 Measures, C.I., and Brown E.T.: Estimating dust input to the Atlantic Ocean using surface water Al
800 concentrations, in, The Impact of desert dust across the Mediterranean, edited by S. Guerzoni and R.
801 Chester, pp.301-311, Kluwer: Dordrecht, 1996.

802 Menzel-Barraqueta, J.-L., Schlosser, C., Planquette, H., Gourain, A., Cheize, M., Boutorh, J., Shelley,
803 R., Pereira Contreira, L., Gledhill, M., Hopwood, M.J., Lherminier, P., Sarthou, G. and Achterberg,
804 E.P. Aluminium in the North Atlantic Ocean and the Labrador Sea (GEOTRACES GA01 section):
805 roles of continental inputs and biogenic particle removal. Biogeosciences Discuss.,
806 <https://doi.org/10.5194/bg-2018-39>, this issue.

807 Morton, P. L., Landing, W.M., Hsu, S.-C., Milne, A., Aguilar-Islas, A.M., Baker, A.R., Bowie, A.R.,
808 Buck, C.S., Gao, Y., Gichuki, S., Hastings, M.G., Hatt, M., Johansen, A. M., Losno, R., Mead, C.,
809 Patey, M.D., Swarr, G., Vandermark, A., Zamora, L.M.: Methods for the sampling and analysis of
810 marine aerosols: results from the 2008 GEOTRACES aerosol intercalibration experiment, Limnology
811 and Oceanography: Methods, 11, 62-78, 2013.

812 Oladottir, B. A., Sigmarsson, O., Larsen, G., and Devidal, J.L.: Provenance of basaltic tephra from
813 Vatnajökull subglacial volcanos, iceland, as determined by major- and trace-element analyses, The
814 Holocene, 21, 1037-1048, [10.1177/0959683611400456](https://doi.org/10.1177/0959683611400456), 2011.

815 Patey, M. D., Achterberg, E.P., Rijkenberg, M.J., and Pearce, R.: Aerosol time-series measurements
816 over the tropical Northeast Atlantic Ocean: Dust sources, elemental, composition and mineralogy,
817 *Marine Chemistry*, 174, 103-119, <http://dx.doi.org/10.1016/j.marchem.2015.06.004>, 2015.

818 Petzold, A., Rasp, K., Weinzierl, B., Esselborn, M., Hamburger, T., Dörnbrack, A., Kandler, K.,
819 Schütz, L., Knippertz, P., Fiebig, M., and Virkkula, A.: Saharan dust absorption and refractive index
820 from aircraft-based observations during SAMUM 2006, *Tellus B*, 61, 118-130, 10.1111/j.1600-
821 0889.2008.00383.x, 2009.

822 Planquette, H., Gourain, A., Cheize, M., Menzel Barraqueta, J.L., Boutorh, J., Shelley, R., Pereira
823 Contreira, L., Lacan, F., Lherminier, P. and Sarthou, G. Particulate trace elements in the North
824 Atlantic along the GEOVIDE section (GEOTRACES GA01), ASLO 2016 Ocean Sciences Meeting,
825 2016.

826 Powell, C. F., Baker, A.R., Jickells, T.D., Bange, H.W., Chance, R.J., Yodle, C.: Estimation of the
827 atmospheric flux of nutrients and trace metals to the eastern tropical North Atlantic Ocean, *Journal of*
828 *the Atmospheric Sciences*, 4029-4045, <http://doi.org/10.1175/JAS-D-15-0011.1>, 2015.

829 Prospero, J. M., Bullard, J.E., and Hodgkins, R.: High-Latitude Dust Over the North Atlantic: Inputs
830 from Icelandic Proglacial Dust Storms, *Science*, 335, 1078-1082,
831 <http://doi.org/10.1126/science.1217447>, 2012.

832 Prospero, J. M., Ginoux, P., Torres, O., Nicholson, S.E. and Thomas, T.E.: Environmental
833 characterization of global sources of atmospheric dust identified with the Nimbus 7 Total Ozone
834 Mapping Spectrometer (TOMS) absorbing aerosol product., *Reviews of Geophysics.*, 40,
835 10.1029/2000RG000095, 2002.

836 Prospero, J. M., Glaccum, R.A. and Nees, R.T.: Atmospheric transport of soil dust from Africa to
837 South America., *Nature.*, 289, 570-572., 570-572., 1981.

838 R Core Team: R: A Language and Environment for Statistical Computing. [https://www.R-](https://www.R-project.org/)
839 [project.org.](https://www.R-project.org/), 2016.

840 Rolph, G.D., Real-time Environmental Applications and Display sYstem (READY) Website
841 (<http://ready.arl.noaa.gov>). NOAA Air Resources Laboratory, Silver Spring, MD, 2017. Rubin, M.,
842 Berman-Frank, I., and Shaked, Y.: Dust- and mineral-iron utilization by the marine dinitrogen-fixer
843 *Trichodesmium*, *Nature Geosci*, 4, 529-534, 2011.

844 Rudnick, R. L., and Gao, S.: Composition of the continental crust, in: *Treatise on Geochemistry*,
845 edited by: Holland, H. D., and Turekian, K.K., Elsevier, Oxford, 1-64, <http://dx.doi.org/10.1016/B0->
846 [08-043751-6/03016-42003](http://dx.doi.org/10.1016/B0-08-043751-6/03016-42003).

847 Rue, E. L., and Bruland, K. W. : Complexation of iron (III) by natural organic ligands in the Central
848 North Pacific as determined by a new competitive ligand equilibrium/ adsorptive cathodic stripping
849 voltammetric method, *Marine Chemistry*, 50, 117-138, 1995.

850 Sarthou, G., Baker, A.R., Blain, S., Achterberg, E.P., Boye, M., Bowie, A.R., Croot, P., Laan, P., de
851 Baar, H.J. W., Jickells, T.D. and Worsfold, P.J.: Atmospheric iron deposition and sea-surface
852 dissolved iron concentrations in the eastern Atlantic Ocean., *Deep Sea Research Part I: Oceanographic*
853 *Research Papers.*, 50, 1339-1352., 2003.

854 Scheuven, D., Schütz, L., Kandler, K., Ebert, M., and Weinbruch, S.: Bulk composition of northern
855 African dust and its source sediments — A compilation, *Earth-Science Reviews*, 116, 170-194,
856 <http://dx.doi.org/10.1016/j.earscirev.2012.08.005>, 2013.

857 Schmidt, K., Schlosser, C., Atkinson, A., Fielding, S., Venables, H.J., Waluda, C.M., and Achterberg,
858 E.P.: Zooplankton gut passage mobilizes lithogenic iron for ocean productivity, *Current Biology*, 26,
859 2667-2673, <https://doi.org/10.1016/j.cub.2016.07.058>, 2016.

860 Sedwick, P. N., Sholkovitz, E.R. and Church, T.M.: Impact of anthropogenic combustion emissions on
861 the fractional solubility of aerosol iron: evidence from the Sargasso Sea., *Geochemistry, Geophysics,*
862 *Geosystems.*, 8, <http://doi.org/10.1029/2007GC001586>, 2007.

863 Sippula, O., Stengel, B., Sklorz, M., Streibel, T., Rabe, R., Orasche, J., Lintelmann, J., Michalke, B.,
864 Abbaszade, G., Radischat, C., Gröger, T., Schnelle-Kreis, J., Harndorf, H., and Zimmermann, R.:
865 Particle Emissions from a Marine Engine: Chemical Composition and Aromatic Emission Profiles
866 under Various Operating Conditions, *Environmental Science & Technology*, 48, 11721-11729,
867 10.1021/es502484z, 2014.

868 Shaked, Y., and Lis, H.: Dissassembling iron availability to phytoplankton, *Frontiers in Microbiology*,
869 3, <http://doi.org/10.3389/fmicb.2012.00123>, 2012.

870 Shelley, R. U., Morton, P.L. and Landing, W.M.: Elemental ratios and enrichment factors in aerosols
871 from the US-GEOTRACES North Atlantic transects, *Deep Sea Research Part II: Topical Studies in*
872 *Oceanography*, 116, 262-272, <http://dx.doi.org/10.1016/j.dsr2.2014.12.005>, 2015.

873 Shelley, R. U., Roca-Martí, M., Castrillejo, M., Sanial, V., Masqué, P., Landing, W.M., van Beek, P.,
874 Planquette, H., and Sarthou, G.: Quantification of trace element atmospheric deposition fluxes to the
875 Atlantic Ocean (> 40°N; GEOVIDE, GEOTRACES GA01) during spring 2014, *Deep Sea Research*
876 *Part I: Oceanographic Research Papers*, 119, 34-49, <http://doi.org/10.1016/j.dsr.2016.11.010>, 2017.

877 Sholkovitz, E., R., Sedwick, P.N. and Church, T.M.: Influence of anthropogenic combustion emissions
878 on the deposition of soluble aerosol iron to the ocean: Empirical estimates for island sites in the North
879 Atlantic., *Geochimica et Cosmochimica Acta.*, 73, 3981-4003., 2009.

880 Sholkovitz, E., R., Sedwick, P.N., Church, T.M., Baker, A.R., and Powell, C.F.: Fractional solubility
881 of aerosol iron: Synthesis of a global-scale data set, *Geochimica et Cosmochimica Acta*, 89, 173-189,
882 2012.

883 Skonieczny, C., Bory, A. Bout-Roumazeilles, V., Abouchami, W., Galer, S. J. G., Crosta, X. Stuut,
884 J.-B., I. Meyer, Chiapello, I., Podvin, T., Chatenet, B., Diallo, A., and Ndiaye, T.: The 7–13 March
885 2006 major Saharan outbreak: Multiproxy characterization of mineral dust deposited on the West
886 African margin, *Journal of Geophysical Research*, 116, <http://doi.org/10.1029/2011JD016173>, 2011.

887 Stein, A.F., Draxler, R.R, Rolph, G.D., Stunder, B.J.B., Cohen, M.D., and Ngan, F.: NOAA's
888 HYSPLIT atmospheric transport and dispersion modeling system, *Bull. Amer. Meteor. Soc.*, 96, 2059-
889 2077, <http://doi.org/10.1175/BAMS-D-14-00110.1>, 2015.

890 Tonnard, M., Planquette, H., Bowie, A.R., van der Merwe, P., Gallinari, M., Desprez de Gésincourt,
891 F., Germain, Y., Gourain, A., Benetti, M., Reverdin, G., Treguer, P., Boutorh, J., Cheize, M., Menzel-
892 Barraqueta, J.L., Pereira-Contreira, L., Shelley, R., Lherminier, P., and Sarthou, G. Dissolved iron in
893 the North Atlantic Ocean and Labrador Sea along the GEOVIDE section (GEOTRACES section
894 GA01), Submitted to *Biogeosciences Discuss.*, this issue.

895 Ussher, S. J., Achterberg, E.P., Powell, C., Baker, A.R., Jickells, T.D., Torres, R., and Worsfold, P.J.:
896 Impact of atmospheric deposition on the contrasting iron biogeochemistry of the North and South
897 Atlantic Ocean, *Global Biogeochemical Cycles*, 27, 1096-1107, <http://doi.org/10.1002/gbc.20056>,
898 2013.

899 Weber, R. J., Guo, H., Russell, A.G., and Nenes, A.: High aerosol acidity despite declining
900 atmospheric sulfate concentrations over the past 15 years, *Nature Geosci*, 9, 282-285,
901 <http://doi.org/10.1038/ngeo2665>

902 Wozniak, A. S., Shelley, R.U., McElhenie, S.D., Landing, W.M., and Hatcher, P.G.: Aerosol water
903 soluble organic matter characteristics over the North Atlantic Ocean: Implications for iron-binding
904 ligands and iron solubility, *Marine Chemistry*, 173, 162-172,
905 <http://dx.doi.org/10.1016/j.marchem.2014.11.002>, 2015.

906 Wozniak, A. S., Shelley, R.U., Sleighter, R.L., Abdulla, H.A.N., Morton, P.L., Landing, W.M., and
907 Hatcher, P.G.: Relationships among aerosol water soluble organic matter, iron and aluminum in
908 European, North African, and Marine air masses from the 2010 US GEOTRACES cruise, *Marine*
909 *Chemistry*, 154, 24-33, <http://dx.doi.org/10.1016/j.marchem.2013.04.011>, 2013.

910 Wozniak, A. S., Willoughby, A. S., Gurganus, S. C., and Hatcher, P. G.: Distinguishing molecular
911 characteristics of aerosol water soluble organic matter from the 2011 trans-North Atlantic US
912 GEOTRACES cruise, *Atmos. Chem. Phys.*, 14, 8419-8434, 10.5194/acp-14-8419-2014, 2014.

913 Zurbrick, C., Boyle, E., Kayser, R., Reuer, M., Wu, J., Planquette, H., Shelley, R., Boutorh, J., Cheize,
914 M., Contreira, L., Menzel, J.L. and Sarthou, G. Dissolved Pb and Pb isotopes in the North Atlantic
915 from the GEOVIDE transect (GEOTRACES GA-01) and heir decadal evolution. *Biogeosciences*
916 *Discuss*, <https://doi.org/10.5194/bg-2018-29>.

917

918

919

920

921

922

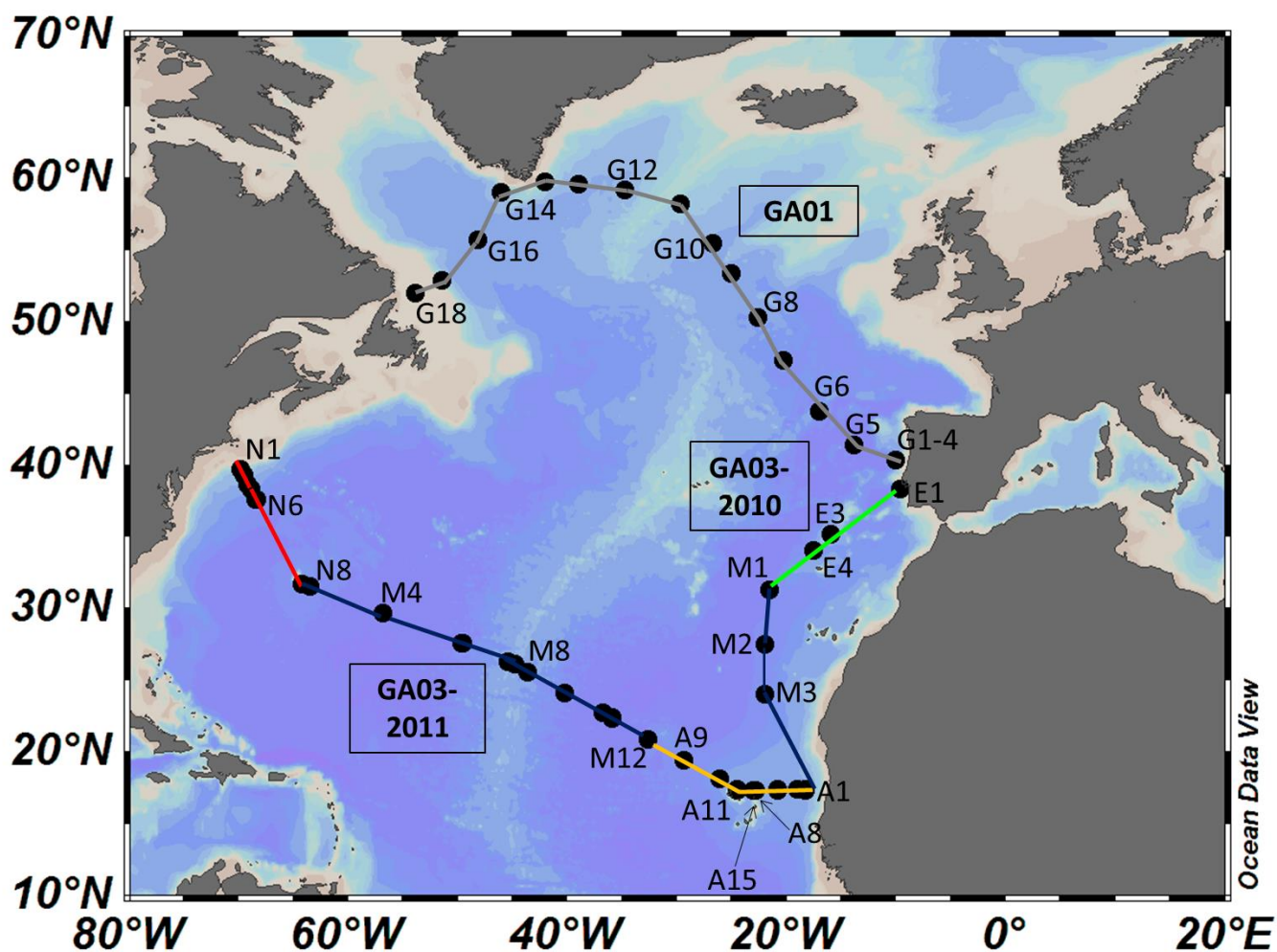


Figure 1

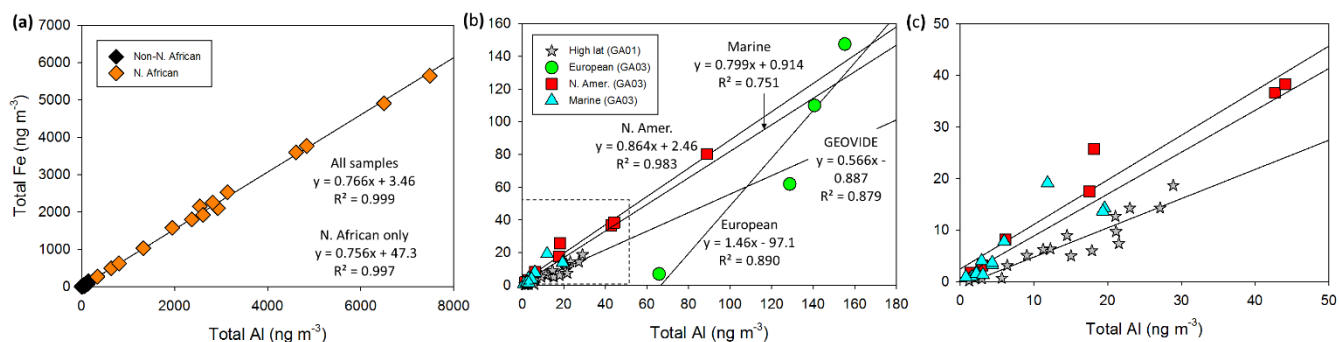


Figure 2

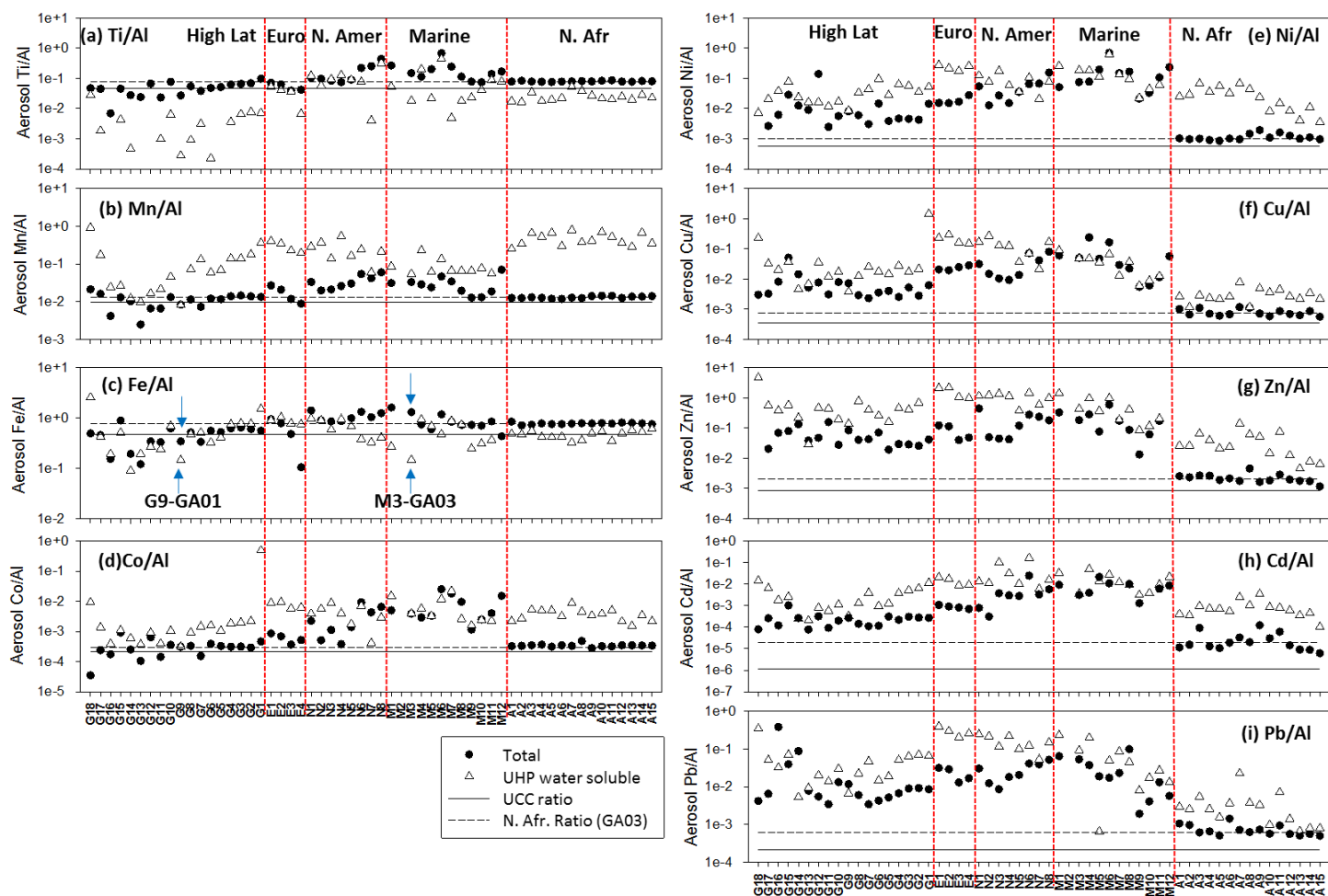


Figure 3

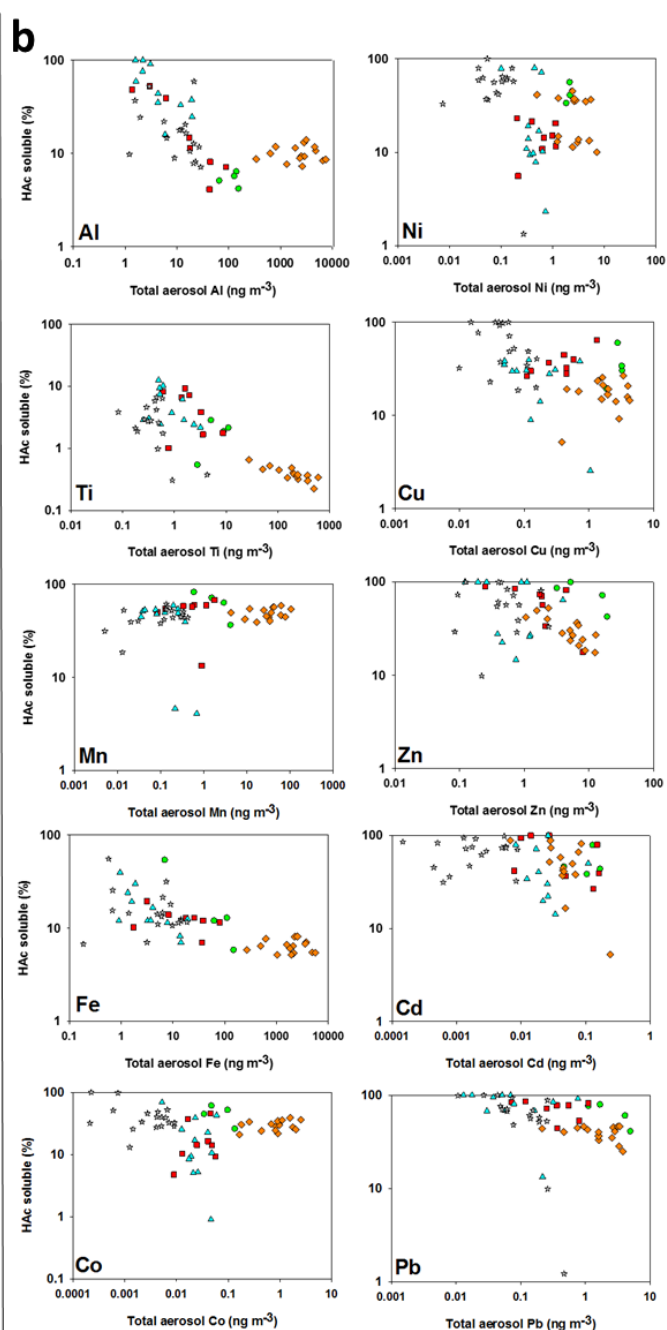
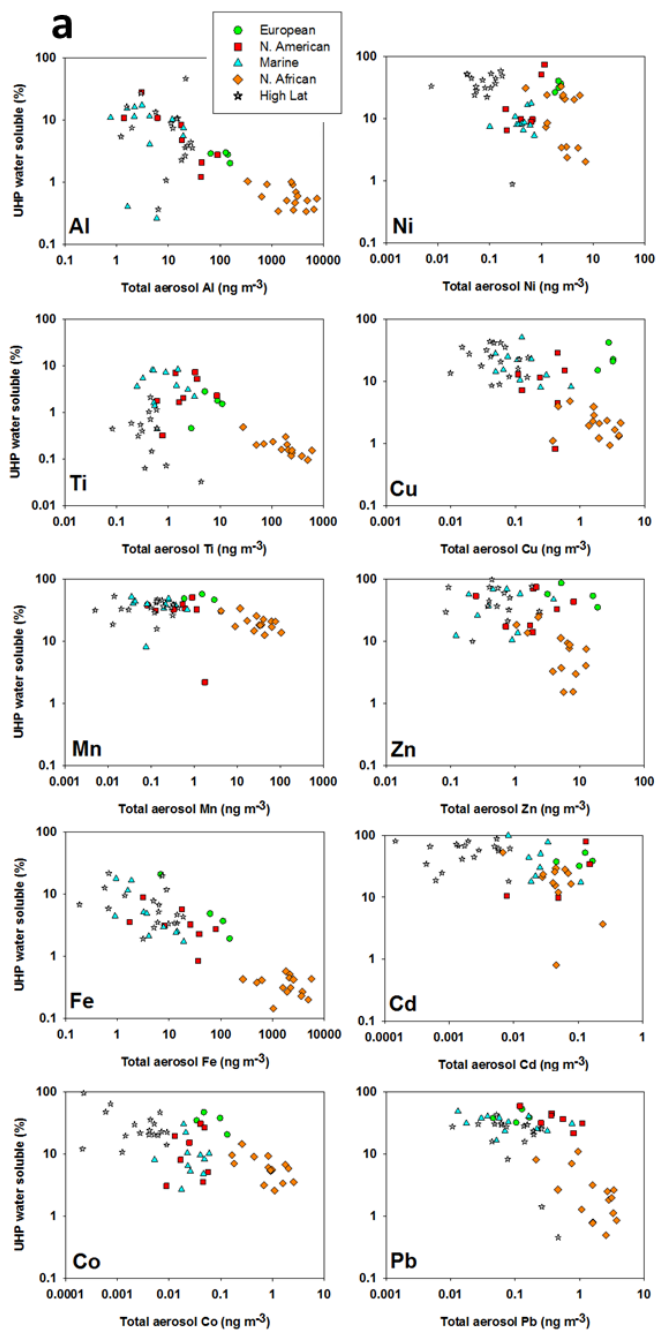
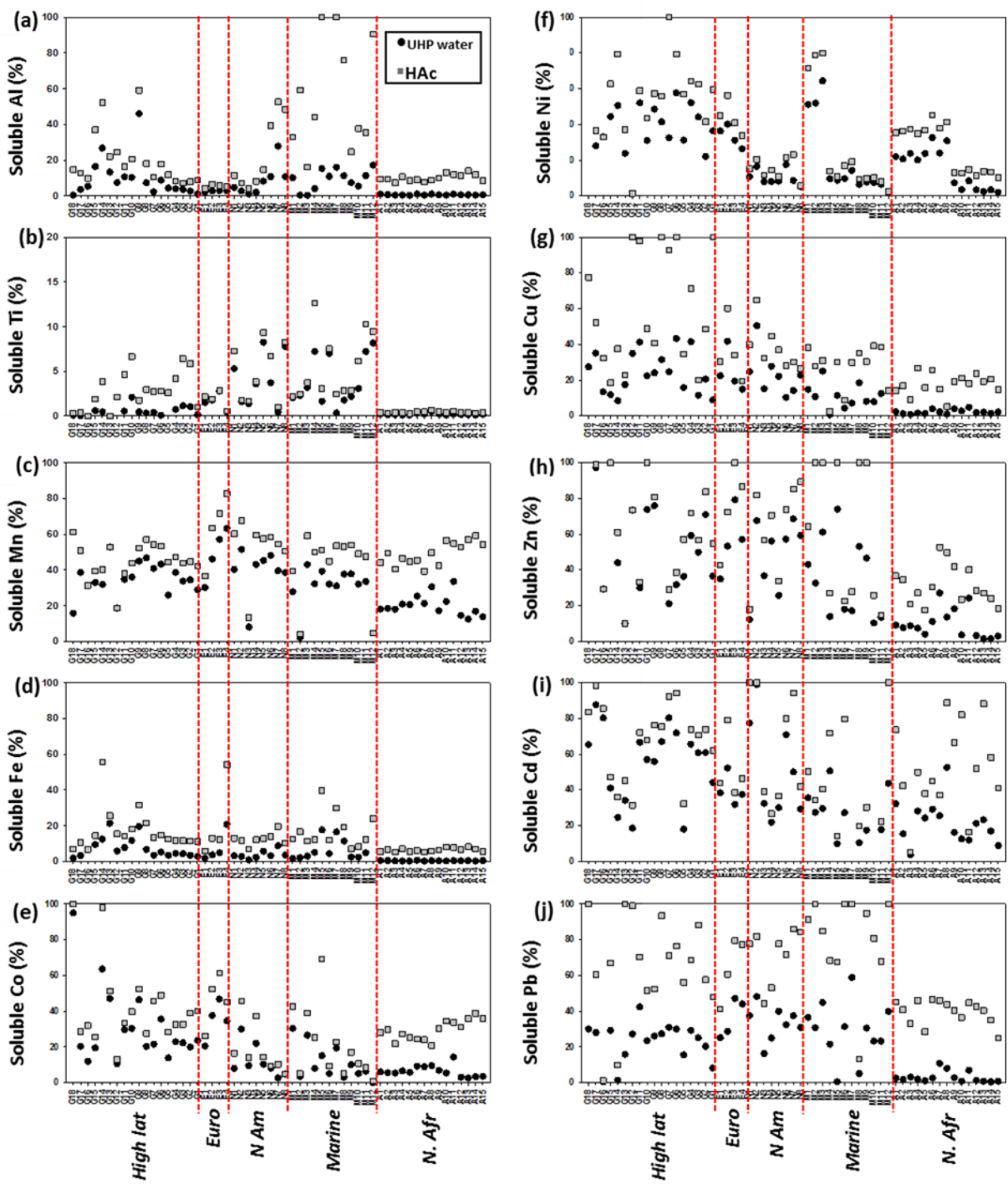


Figure 4



951

952 **Figure 5**

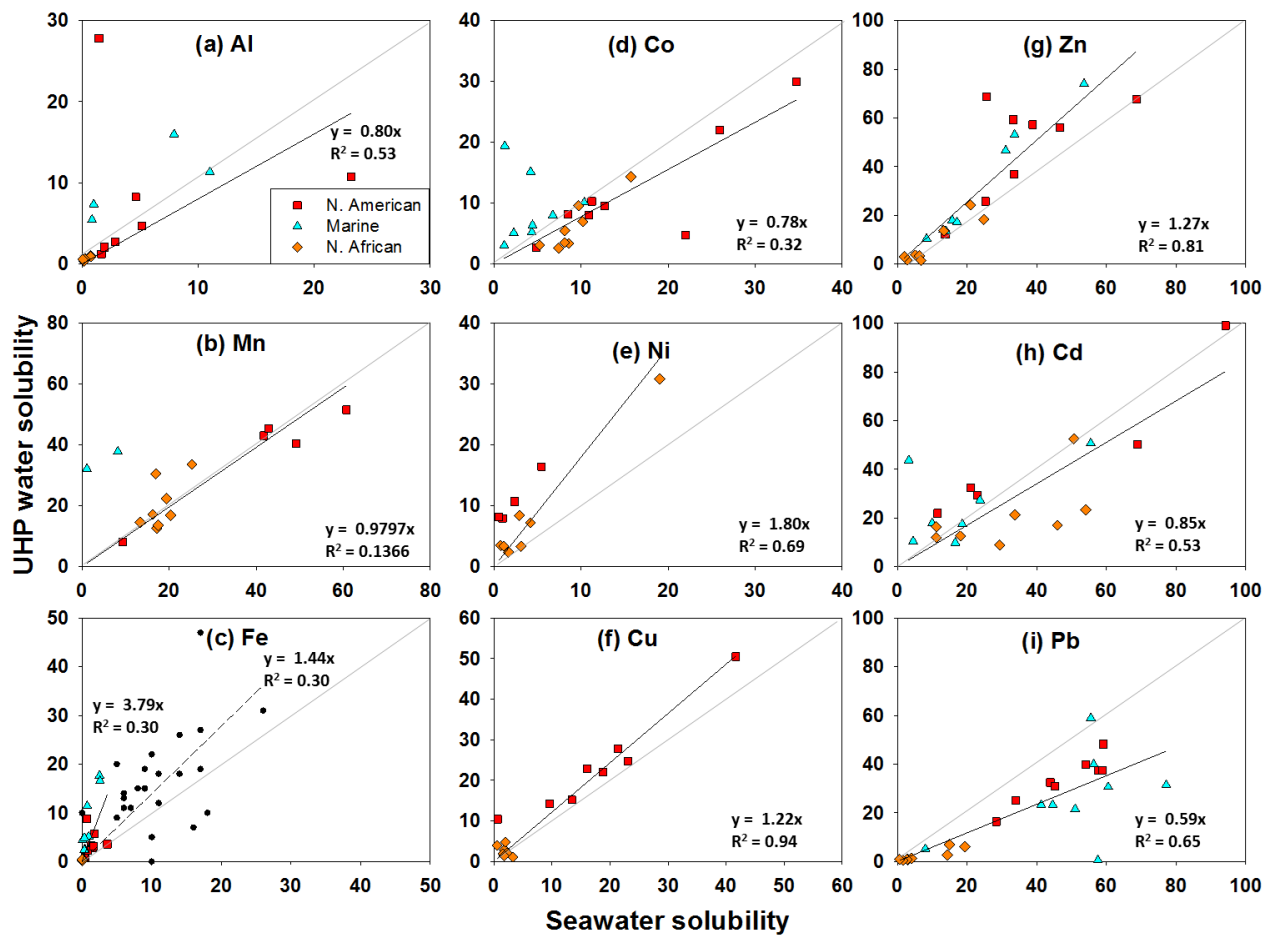


Figure 6

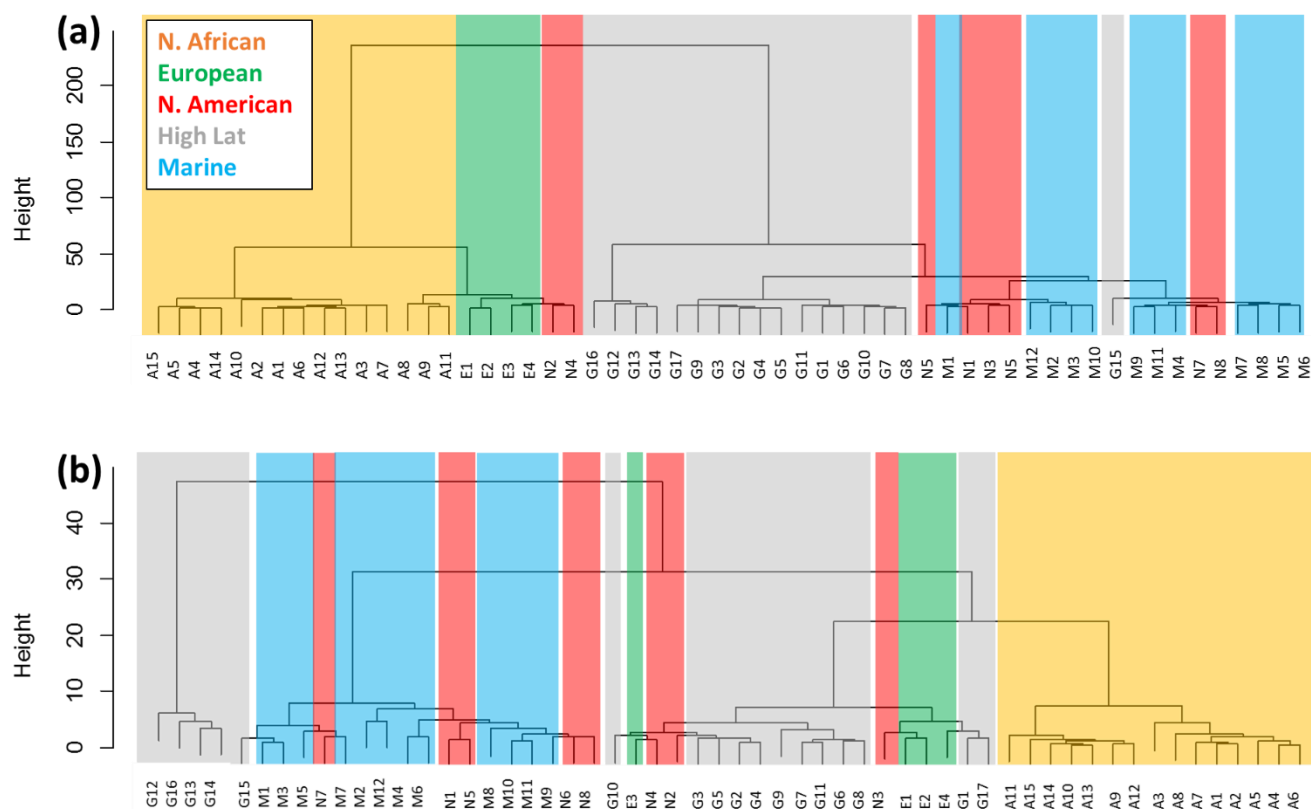


Figure 7

Captions: Figures

Figure 1. The GEOTRACES GA01 and GA03 cruise tracks (GA01, GA03-2010 and GA03-2011). In total, 57 aerosol samples (GA01 $n = 18$, GA03 $n = 39$; black dots) were collected. The samples are grouped by aerosol source region (green = European (E1-4), blue = Marine (M1-12), yellow = North African (A1-15), red = North American (N1-8), and grey = High Latitude (G1-18)), identified from air mass back trajectory simulations using the NOAA ARL model, HYSPLIT (Stein et al., 2015; Rolph, 2017). Note that a different labelling convention was used in Shelley et al. (2017) to refer to the GA01 samples. Here we use G1-18 to refer to the samples collected during GA01 (A1-18 in Shelley et al., 2017), and A1-15 to refer to the North African samples from GA03.

Figure 2. Total aerosol Fe and Al (ng m^{-3}) for: (a) all aerosol samples from cruises GA01 and GA03, (b) samples from sources other than North Africa (i.e. the black diamonds in Fig. 2a), and (c) the samples inside the dashed box in Fig. 2b. For High Latitude dust $n = 18$, European samples $n = 4$, North American samples $n = 8$, Marine samples $n = 12$, and Saharan samples $n = 15$. Note error bars (standard deviations shown in Table S1) are not included so as not to obscure the symbols.

Figure 3. Elemental mass ratios (normalised to Al) of total (black circles) and UHP water soluble (white triangles) TEs. The UCC elemental ratio (Rudnick and Gao, 2003) is indicated by the solid horizontal line, and the elemental ratio in North African sourced aerosols (Shelley et al., 2015) is indicated by the dashed horizontal

996 line on each plot. The red vertical lines separate the aerosol source regions, which are labelled in panel (a).
997 Samples G9-GA01 and M3-GA03 are indicated by blue arrows in panel c (see text for details).
998
999 Figure 4. (a) Percentage of UHP water soluble TE (calculated from Eq. 1) versus total aerosol TE (ng m^{-3}), (b)
1000 percentage of 25 % acetic acid soluble TE (calculated from Eq. 2) versus total aerosol TE (ng m^{-3}). Data is
1001 plotted on log-log scales.
1002
1003 Figure 5. Solubility of Al, Ti, Mn, Fe, Co, Ni, Cu, Zn, Cd, Pb following a UHP water leach (UHP water, black
1004 circles, calculated using Eq. 1), and a sequential leach of 25 % acetic acid (HAc, grey squares, calculated using
1005 Eq. 2). The red vertical dashed lines represent the different aerosol source categories, as labelled in panel (b).
1006 Note that Ti (panel b) is highly insoluble and has a maximum value of <13%. The data for this figure is also
1007 presented in Fig. S4 as biplots of UHP water fractional solubility versus 25 % acetic acid fractional solubility.
1008
1009 Figure 6. Comparison of TE solubility following instantaneous leaches using UHP water or locally-collected,
1010 filtered seawater. The solid line is the 1:1 line. Where fewer data are observed, concentrations were below
1011 detection for one or both of the two leaches. The data for soluble aerosol Fe from within our study region from
1012 Buck et al. (2010) are plotted as black circles in panel (c).
1013
1014 Figure 7. Hierarchical cluster analysis of (a) log transformed total TE concentration data plus NO_3^-
1015 concentration data, and (b) log transformed fractional solubility following the two-step sequential leach
1016 (fractional solubility calculated using Eq. 2) plus NO_3^- concentration data. The coloured blocks correspond with
1017 the aerosol source regions shown in the legend (note that the North African samples correspond with the yellow
1018 blocks of colour).
1019
1020
1021
1022